Some stationary properties of a *Q*-ball in arbitrary space dimensions

Mitsuo I. Tsumagari,[*] Edmund J. Copeland,[+] and Paul M. Saffin[‡]

School of Physics and Astronomy, University of Nottingham, University Park, Nottingham NG7 2RD, United Kingdom
(Received 17 June 2008; published 11 September 2008)

Introducing new physically motivated ansätze, we explore both analytically and numerically the classical and absolute stabilities of a single *Q*-ball in an arbitrary number of spatial dimensions *D*, working in both the thin- and thick-wall limits.

I. INTRODUCTION

In a pioneering paper published in 1985 [1], Sidney Coleman showed that it was possible for a new class of nontopological solitons [2] to exist within a self-interacting system by introducing the notion of a *Q*-ball. His model had a continuous unbroken global U(1) charge *Q* (for reviews see [3–6]), which corresponds to an angular motion with angular velocity ω in the U(1) internal space. The conserved charge stabilizes the *Q*-ball, unlike the case of topological solitons whose stability is ensured by the presence of conserved topological charges. Once formed, a *Q*-ball is absolutely stable if four conditions are satisfied: (1) *existence condition* [1]—its potential should grow less quickly than the quadratic mass term, and this can be realized through a number of routes such as the inclusion of radiative or finite temperature corrections to a bare mass, or nonlinear terms in a polynomial potential [1,7], (2) *absolute stability condition*—the energy E_Q (or mass) of a *Q*-ball must be lower than the corresponding energy that the collection of the lightest possible scalar particle quanta (rest mass *m*) could have, (3) *classical stability condition* [2]—the *Q*-ball should be stable to linear fluctuations, with the threshold of the stability being located at the saddle point of the *D*-dimensional Euclidean action, the bounce action S_ω [8], (4) *fission condition* [3]—the energy of a single *Q*-ball must be less than the total energy of the smaller *Q*-balls into which it could, in principle, fragment. It turns out that for each of the four conditions to be satisfied we require

$$\omega_- \lesssim |\omega| < \omega_+, \qquad E_Q < mQ,$$

$$\frac{\omega}{Q}\frac{dQ}{d\omega} \leq 0 \Leftrightarrow \frac{d^2 S_\omega}{d\omega^2} \geq 0, \qquad \frac{d^2 E_Q}{dQ^2} < 0 \Leftrightarrow \frac{d\omega}{dQ} < 0 \qquad (1)$$

where $\omega_\mp$ are the lower and upper limits of ω that the *Q*-ball can have. The lower limit, $\omega \simeq \omega_-$, can define thin-wall *Q*-balls, either without [1] or with [9,10] the wall thickness being taken into account, while the upper limit,

$\omega \simeq \omega_+$, can define thick-wall *Q*-balls in [11] which may be approximated by a simple Gaussian ansatz [12].

There is a vast amount of literature on nontopological solitons, including *Q*-balls. They have been seen to be solutions in Abelian gauge theories [10,13–17], in non-Abelian theories [18–20], in self-dual (Maxwell-) Chern-Simons theory [21–24], in noncommutative complex scalar field theory [25], in models which include fermionic interactions [13–15,17,26,27], as well as in the presence of gravity [28,29]. *Q*-balls themselves have been quantized either by canonical [2] or by path integral schemes [30–32]. With thermal effects, it has been shown that *Q*-balls coupled to massless fermions are able to evaporate away [33]; however, at sufficiently low temperatures they become stable, and indeed they then tend to grow [34,35]. The authors in [2,10,36,37] have discussed and analyzed the spatially excited states of *Q*-balls, including radial modes as well as spatially dependent phase excitations. A more general mathematical argument concerning the stability of solitary waves can be found in [38,39]. A class related to *Q*-balls consists of objects known as oscillons [40–42] or as I-balls [43], and recent attention has turned to the dynamics of these time-dependent, nonlinear, metastable configurations [44–46].

Standard *Q*-balls exist in an arbitrary number of space dimensions *D* and are able to avoid the restriction arising from Derrick's theorem [47] because they are time-dependent solutions. A few examples include polynomial models both for $D = 3$ [48,49] and for arbitrary *D* [12]; models with supersymmetry broken by gravity mediation [49]; and models with supersymmetry broken by gauge interaction [35,50,51]. Returning to the case of $D = 3$, phenomenologically, it turns out that the *Q*-balls present in models with gravity mediated supersymmetry breaking are quasistable but long-lived, allowing, in principle, for these *Q*-balls to be the source of both the baryons and the lightest supersymmetric particle (LSP) dark matter particle [52]. On the other hand, *Q*-balls in models of gauge mediated supersymmetry breaking can be dark matter candidates, as they can be absolutely stable [6]. Both types of *Q*-balls have been shown to be able to provide the observed baryon-to-photon ratio [35].

The dynamics and formation of *Q*-balls involve solving complicated nonlinear systems, which generally require

[*]ppxmt@nottingham.ac.uk
[+]ed.copeland@nottingham.ac.uk
[‡]paul.saffin@nottingham.ac.uk

numerical simulations. The dynamics of two Q-balls in flat Minkowski space-time depends on parameters such as the relative phases between them and the relative initial velocities [7,50,53]. In addition, the main formation process through the Affleck-Dine mechanism [54] has been extensively examined in gauge mediated [55], gravity mediated [56–58], and running inflaton mass models [59]. As analyzing individual Q-balls is difficult in its own right, it is extremely challenging to deal with multiple Q-balls. A number of analytical approaches to address that issue have been made over the past few years, e.g. [60–62]. Multiple thermal Q-balls have been described in a statistical sense in [57,63].

In this paper we aim to analytically and numerically address stationary properties of a single Q-ball in an arbitrary number of spatial dimensions. This work will draw on earlier work of Correia and Schmidt [30] who derived analytic properties for the thin- and thick-wall limits of Q-balls in $D = 3$. Recently, Gleiser and Thorarinson [12] proved the absolute stability for thin-wall Q-balls using the virial theorem. We will generalize the main results of [12,30] to the case of arbitrary spatial dimensions, and in doing so, will both analytically predict and numerically confirm the unique values of the angular velocity ω_a for the absolute stability of the Q-balls via both the virial relation and thin-wall Q-ball approximations.

Moreover, we will obtain the classical stability conditions for the thin- and thick-wall approximations, and discover the connections between the virial relation and the thin- or thick-wall approximation for the characteristic slopes $E_Q/\omega Q$. In a companion paper [64] we will investigate dynamical properties of multiple Q-balls, including thermal effects, and their formation (see [65] for movies showing the dynamics of single Q-balls).

This paper is divided into the following sections. In Sec. II we review the properties of a Q-ball in an arbitrary number of spatial dimensions D, including the existence and stability conditions. By introducing a number of different ansätze, in Sec. III we present a detailed analysis of the solutions in the thin- and thick-wall limits. We then demonstrate the advantages of using two particular modified ansätze in Sec. IV, where we present detailed numerical results for the case of both degenerate and nondegenerate underlying potentials. Finally, we conclude in Sec. V.

II. Q-BALL IN D DIMENSIONS

We shall begin with a standard Q-ball ansatz [1] which satisfies a Laplace equation, called the Q-ball equation, and we will introduce the Legendre relations [2] which will make some computations easier. The existence of Q-balls places constraints on the allowed form of the potential, and introduces limiting values of ω, i.e. $\omega_\pm$, near which we may describe the Q-balls analytically using either a thick- or thin-wall approximation. We will then introduce three conditions for Q-balls to be stable [3]. Finally, we will

obtain the characteristic slope $E_Q/\omega Q$ and minimum charge $Q_{\min}$, and propose approximate values for ω_a, the limiting frequency for absolute stability, using a virial theorem and showing that it does not rely on detailed analytic profiles and potential forms.

A. Q-ball ansatz

We consider a complex scalar field ϕ in Minkowski space-time of arbitrary spatial dimensions D with a U(1) potential bounded by $U(|\phi|) \geq 0$ for any values of ϕ:

$$S = \int d^{D+1}x\sqrt{-g}\mathcal{L}, \qquad (2)$$

where

$$\mathcal{L} = -\tfrac{1}{2}g^{\mu\nu}\partial_\mu\phi^\dagger\partial_\nu\phi - U(|\phi|). \qquad (3)$$

The metric is $ds^2 = g_{\mu\nu}dx^\mu dx^\nu = -dt^2 + h_{ij}dx^i dx^j$ and g is the determinant of $g_{\mu\nu}$ where μ, ν run from 0 to D, and i, j denote spatial indices running from 1 to D. Now, using the standard decomposition of ϕ in terms of two real fields $\phi = \sigma e^{i\theta}$, the energy momentum tensor $T_{\mu\nu} \equiv -\frac{2}{\sqrt{-g}} \times \frac{\delta S}{\delta g_{\mu\nu}} +$ (symmetrizing factors) and the conserved U(1) global current $j_{\mu,U(1)}$ via the Noether theorem, we obtain

$$T_{\mu\nu} = (\partial_\mu\sigma\partial_\nu\sigma + \sigma^2\partial_\mu\theta\partial_\nu\theta) + g_{\mu\nu}\mathcal{L}, \qquad (4)$$

$$j_{\mu,U(1)} = \sigma^2\partial_\mu\theta. \qquad (5)$$

Using a basis of vectors $\{n^\mu_{(a)}\}$ where $n^\mu_{(t)}$ is timelike and $n^\mu_{(i)}$ are spacelike unit vectors oriented along the spatial i direction, the above currents give the definitions of energy density ρ_E, charge density ρ_Q, momentum flux $\hat{P}_i$, and pressure p:

$$\begin{aligned} \rho_E &\equiv T_{\mu\nu}n^\mu_{(t)}n^\nu_{(t)}; & \rho_Q &\equiv j_\mu n^\mu_{(t)}; \\ \hat{P}_i &\equiv T_{\mu\nu}n^\mu_{(t)}n^\mu_{(i)}; & p &\equiv T_{\mu\nu}n^\mu_{(i)}n^\nu_{(i)}. \end{aligned} \qquad (6)$$

Defining the D-dimensional volume V_D bounded by a $(D-1)$-sphere, the Noether charges [energy, momenta, and U(1) charges] become

$$E = \int_{V_D}\rho_E, \qquad P_i = \int_{V_D}\hat{P}_i, \qquad Q = \int_{V_D}\rho_Q, \quad (7)$$

where $\int_{V_D} \equiv \int d^D x\sqrt{h}$. Minimizing an energy with a fixed charge Q for any degrees of freedom, we find the Q-ball (lowest) energy E_Q by introducing a Lagrange multiplier ω and setting $n^\mu_t = (-1, 0, 0, \ldots, 0)$:

$$E_Q = E + \omega\Big(Q - \int_{V_D}\rho_Q\Big), \qquad (8)$$

$$= \omega Q + \int_{V_D} \left(\frac{1}{2} \{ \dot{\sigma}^2 + \sigma^2 (\dot{\theta} - \omega)^2 + (\nabla\sigma)^2 + \sigma^2 (\nabla\theta)^2 \} \right.$$
$$\left. + U_\omega \right), \qquad (9)$$

$$= \omega Q + S_\omega \qquad (10)$$

where $U_\omega = U - \frac{1}{2}\omega^2\sigma^2$, $\dot{\sigma} \equiv \frac{d\sigma}{dt}$ etc., and ω will turn out to be the rotation frequency in the U(1) internal space. The presence of the positive definite terms in Eq. (9) suggests that the lowest energy solution is obtained by setting $\dot{\sigma} = 0 = \dot{\theta} - \omega = \nabla\theta$. The Euclidean action S_ω and the effective potential U_ω in Eqs. (9) and (10) are finally given by

$$S_\omega = \int_{V_D} \frac{1}{2}(\nabla\sigma)^2 + U_\omega, \qquad U_\omega \equiv U - \frac{1}{2}\omega^2\sigma^2. \quad (11)$$

The second term in U_ω comes from the internal spin of the complex field. Following Friedberg *et al.* [2], it is useful to define the functional

$$G_I \equiv \int_{V_D} \frac{1}{2}(\nabla\sigma)^2 + U = E_Q - \left(\frac{1}{2}\omega^2\right)I$$

$$= S_\omega + \left(\frac{1}{2}\omega^2\right)I \qquad (12)$$

where $\frac{1}{2}\omega^2$ is the corresponding Lagrange multiplier and $I \equiv \int_{V_D} \sigma^2$.

Given that the spherically symmetric profile is the minimum energy configuration [66], we are led to the standard stationary Q-ball ansatz

$$\phi = \sigma(r)e^{i\omega t}. \qquad (13)$$

Substituting Eq. (13) into Eq. (6), we find

$$\rho_E = \frac{1}{2}\sigma'^2 + U + \frac{1}{2}\sigma^2\omega^2, \qquad \rho_Q = \omega\sigma^2, \qquad (14)$$

$$p_r = \frac{1}{2}\sigma'^2 - U_\omega, \qquad P_i = 0 \qquad (15)$$

where $\sigma' \equiv \frac{d\sigma}{dr}$ and p_r is the radial pressure given in terms of the radially oriented unit vector $n_s^\mu = (0, 1, 0, \ldots, 0)$. Without loss of generality, we set both ω and Q as positive.

B. Legendre relations

It is sometimes difficult to compute E_Q directly, but using Legendre relations often helps [2,30]. In our case, from Eq. (10) and (12) we find

$$\frac{dE_Q}{dQ}\bigg|_{S_\omega} = \omega, \qquad \frac{dS_\omega}{d\omega}\bigg|_{E_Q} = -Q, \qquad \frac{dG_I}{dI}\bigg|_{S_\omega} = \frac{1}{2}\omega^2$$
$$(16)$$

because Q-ball solutions give the extrema of E_Q, S_ω, and G_I as regards Q, ω, and I, respectively. These variables match the corresponding "thermodynamic" ones: E_Q, ω, Q, S_ω, and G_I correspond to the internal energy, chemical potential, particle number, and thermodynamic potentials

[35]. After computing S_ω or G_I, one can calculate Q or $\frac{1}{2}\omega^2$ using the second or third relation in Eq. (16), and can compute E_Q using Eq. (10) or Eq. (12), i.e.

$$S_\omega \to Q = -\frac{dS_\omega}{d\omega} \to E_Q = \omega Q + S_\omega, \qquad (17)$$

or similarly $G_I \to \frac{1}{2}\omega^2 = \frac{dG_I}{dI} \to E_Q = G_I + (\frac{1}{2}\omega^2)I$, $S_\omega = G_I - (\frac{1}{2}\omega^2)I$. We shall make use of this powerful technique later.

C. Q-ball equation and existence condition

Let us consider the action $S = -\int dt S_\omega$ in Eq. (2) with our ansatz Eq. (13) and the following boundary condition on a $(D-1)$-sphere which represents spatial infinity,

$$\sigma'| = 0 \text{ on the } (D-1)\text{-sphere.} \qquad (18)$$

Varying S_ω with respect to σ we obtain the Q-ball equation:

$$\frac{d^2\sigma}{dr^2} + \frac{D-1}{r}\frac{d\sigma}{dr} - \frac{dU_\omega}{d\sigma} = 0, \qquad (19)$$

$$\Leftrightarrow \frac{d}{dr}\left(\frac{1}{2}\left(\frac{d\sigma}{dr}\right)^2 - U_\omega\right) = -\frac{D-1}{r}\left(\frac{d\sigma}{dr}\right)^2 \le 0. \quad (20)$$

There is a well-known mechanical analogy for describing the Q-ball solution of Eq. (19) [1], and that comes from viewing Eq. (19) in terms of the Newtonian dynamics of a unit-mass particle with position σ, moving in potential $-U_\omega$ with a friction $\frac{D-1}{r}$, where r is interpreted as a time coordinate. Moreover, $\rho_Q = \omega\sigma^2$ can be considered as the angular momentum.[1] Note that the friction term is proportional to $\frac{D-1}{r}$, and hence becomes significant for high D and/or small r. According to Eq. (20), the "total energy," $\frac{1}{2}(\frac{d\sigma}{dr})^2 - U_\omega$, is conserved for $D = 1$ and/or $r \to \infty$, implying that in that limit the Q-balls have no radial pressure. Of course these are really field theory objects, and consequently, more restrictions apply: (i) no symmetry breaking, in other words $\sigma(r \to \text{large}) = 0$, $U''(\sigma = 0) \equiv m^2 > 0$ with an effective mass m, (ii) regularity condition, $\sigma'(r = 0) = 0$, (iii) reflection symmetry under $\sigma \to -\sigma$. Note that Eq. (19) coupled with the boundary condition Eq. (18) implies that $\sigma(r)$ is a monotonically decreasing function, i.e. $\sigma' < 0$. In fact, according to Eqs. (18) and (19) and the above conditions, our mechanical analogy implies that a static particle with a unit mass should be released somewhere on its potential, eventually reaching the origin at large (but finite) time and stopping there due to the presence of a position- and D-dependent friction. These requirements constrain the allowed forms of the U(1) potentials: for example, if the local maximum of the effective potential $-U_\omega$ is less than 0, the "particle" cannot

---

[1]I is realized as an inertia moment in this mechanical analogy [1,2].

reach the origin, a process known as *undershooting*. To avoid undershooting we require

$$\max(-U_\omega) \geq 0 \Leftrightarrow \min\left(\frac{2U}{\sigma^2}\right) \leq \omega^2. \tag{21}$$

If $-U_\omega$ is convex at $\sigma = 0$, the particle cannot stop at the origin, a situation termed *overshooting*, such that

$$\frac{d^2 U_\omega}{d\sigma^2}\bigg|_{\sigma=0} < 0 \Leftrightarrow \omega^2 < \frac{d^2 U}{d\sigma^2}\bigg|_{\sigma=0}. \tag{22}$$

Combining Eqs. (21) and (22), we find the condition on ω for the existence of a single Q-ball:

$$\omega_- \leq |\omega| < \omega_+ \tag{23}$$

where we have defined the lower and upper bounds of ω as $\omega_\mp$, i.e. $\omega_-^2 \equiv \min(\frac{2U}{\sigma^2}) \geq 0$ and $\omega_+^2 \equiv \frac{d^2 U}{d\sigma^2}|_{\sigma=0} = m^2$. The case $\omega_- = 0$ corresponds to degenerate vacua potentials (DVPs), while the other case, $\omega_- \neq 0$, does not have degenerate vacua (NDVPs). The *existence condition* in Eq. (23) shows that U(1) potentials must have a nonlinear interaction and U_ω is weakly attractive [3]. For convenience, we define the maximum of the effective potential to be at σ_+ (i.e. $\frac{dU_\omega}{d\sigma}|_{\sigma=\sigma_+} = 0$); thus, $\omega_-^2 = \frac{2U_+}{\sigma_+^2}$ and $U_{\omega_-}(\sigma_+) = 0$. Moreover, σ_- satisfies $U_\omega(\sigma_-) = 0$ for $\sigma_- \neq 0$. Notice that $\sigma_- \simeq \sigma_+$ when $\omega \simeq \omega_-$. In Fig. 1, we indicate the above-introduced parameters, $\sigma_\pm$, ω_-, using typical original and effective potentials for both DVP (left panel) and NDVP (right panel). To proceed with analytical arguments, we consider the two limiting values of ω or $\sigma_0 \equiv \sigma(0)$ which describe

$$\begin{cases} \bullet \quad \text{thin-wall } Q\text{-balls when } \omega \simeq \omega_- \text{ or } \sigma_0 \simeq \sigma_+ \\ \bullet \quad \text{thick-wall } Q\text{-balls when } \omega \simeq \omega_+ \text{ or } \sigma_0 \simeq \sigma_-. \end{cases}$$
$$\tag{24}$$

We will not be considering Q-ball solutions that exist in a false vacua where $\omega_-^2 < 0$ [9] or in flat potentials. When it comes to obtaining Q-ball profiles numerically, we will adopt a standard shooting method which fine-tunes the "initial positions" σ_0 subject to $\sigma_-(\omega) \leq \sigma_0 < \sigma_+(\omega)$, in order to avoid *undershooting* and *overshooting*.

D. Three kinds of stability

1. Absolute stability

When the volume V_D approaches infinity [3] and/or ω is outside the limits of Eq. (23), then plane wave solutions can exist around the vacua of $U(|\phi|)$. The equation of motion for ϕ becomes a free Klein-Gordon equation whose solution can be written as $\phi = Ne^{i(\mathbf{k}\cdot\mathbf{x} - \omega_k t)}$ where $\omega_k = \sqrt{m^2 + \mathbf{k}^2}$ and the normalization factor $N = \sqrt{\frac{Q}{2\omega_k V_D}}$ has been calculated from Q. Then the energy of the plane wave solution is proportional to ω_k and Q linearly: $E_{\text{free}} = \omega_k Q \rightarrow E_{\text{free}} \simeq mQ$ where we have taken the infrared limit to obtain the second relation. The energy E_{free} can be interpreted as the energy of a number Q of free particle quanta with rest mass m. Furthermore, one might expect that the thick-wall Q-ball energy with $\omega \simeq \omega_+ = m$ approaches E_{free} because the Q-ball profiles approach zero exponentially at infinity [3]:

$$E_Q(\omega = \omega_+) \simeq E_{\text{free}} \simeq mQ. \tag{25}$$
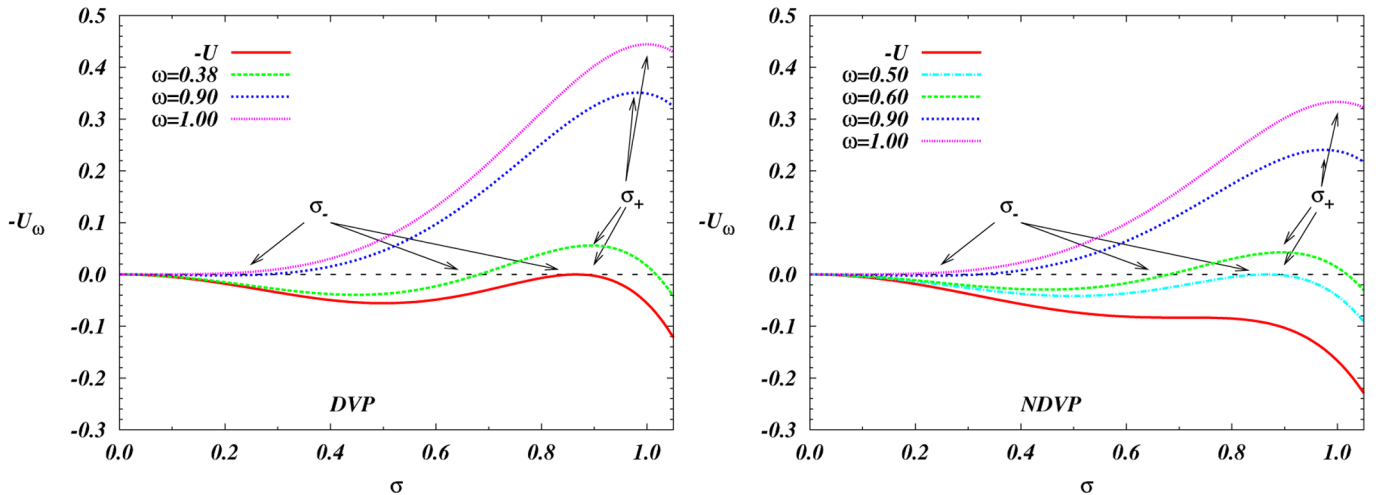

FIG. 1 (color online). Parameters $\sigma_\pm$ in two typical potentials $U(\sigma) = \frac{1}{2}\sigma^2 - A\sigma^4 + B\sigma^6$ where $m = \omega_+ = 1$ and the effective potentials $-U_\omega$ are plotted for various values of ω: DVP with $A = \frac{4}{3}$, $B = \frac{8}{9}$ in the left panel, and NDVP with $A = 1$, $B = \frac{2}{3}$ in the right panel. The DVP has degenerate vacua in the original potential $-U$ (red solid line) where we set $\omega_- = 0$. The NDVP does not have degenerate vacua, but with $\omega = \omega_- = 0.5$ (sky-blue dot-dashed line) the effective potential $-U_\omega$ does have degenerate vacua. The two lines in the lower limit $\omega = \omega_-$ show that $\sigma_- \rightarrow \sigma_+$, where we have defined the maximum of the effective potential to be at σ_+ and $U_\omega(\sigma_-) = 0$ for $\sigma_- \neq 0$. The purple lines show $\sigma_- \rightarrow 0$ with the thick-wall limit $\omega = \omega_+$. With some values of ω (green dotted lines) satisfying the existence condition Eq. (19), both potentials show the values of $\sigma_\mp$ clearly.

Hence the *absolute stability* condition for a *Q*-ball becomes

$$E_Q(\omega) < E_{\text{free}}. \tag{26}$$

We would expect Eq. (26) to be the strongest condition which a *Q*-ball solution has to satisfy.

2. Classical stability

The *classical stability* [2,3] can be defined in terms of the mass squared of the fluctuations around a *Q*-ball solution. For zero mass fluctuations this corresponds to a zero mode, i.e. translation and phase transformation of the *Q*-ball solution. Using collective coordinates and Eq. (19), which extremizes S_ω, such a mode can be removed. Since a detailed analysis can be found in the literature [2,3], we simply state the final result which implies that the *classical stability* condition is

$$\frac{\omega}{Q}\frac{dQ}{d\omega} \leq 0 \Leftrightarrow \frac{d^2 S_\omega}{d\omega^2} \geq 0 \tag{27}$$

where we have used Eq. (16) in the second relation of Eq. (27). Since ω and Q have the same sign, the sign of $\frac{dQ}{d\omega}$ signals whether the solution is classically stable. The first relation of Eq. (27) indicates the presence of an extreme charge in the parameter space of ω (we will later see that the extreme charge at some critical value $\omega = \omega_c$ turns out to be the minimum allowed and will be denoted by $Q_{\min}$). Let us remark on the characteristic slope of E_Q/Q as a function of ω:

$$\frac{d}{d\omega}\left(\frac{E_Q}{Q}\right) = -\frac{S_\omega}{Q^2}\frac{dQ}{d\omega} \geq 0 \tag{28}$$

where we have used Eqs. (10) and (16). Since, as we will see, $S_\omega > 0$ for all possible values of ω within Eq. (23) (in a specific potential [67]), the classically stable *Q*-balls should satisfy $\frac{d}{d\omega}(\frac{E_Q}{Q}) \geq 0$. The conditions from both Eqs. (27) and (28) must be the same.

3. Stability against fission

Suppose the total energy of two *Q*-balls is less than the energy of a single *Q*-ball carrying the same total charge. The single *Q*-ball naturally decays into two or more *Q*-balls with some release of energy. As shown in [3], the stability condition against *fission* for a *Q*-ball is given by

$$\frac{d^2 E_Q}{dQ^2} < 0 \Leftrightarrow \frac{d\omega}{dQ} < 0 \tag{29}$$

where we have used Eq. (16) in the second relation of Eq. (29). Note that this is the same condition as we found above in Eqs. (27) and (28), so the condition for classical stability is identical to that of stability against fission.

Trying to summarize the stability, we can categorize three types of *Q*-balls: i.e. absolutely stable, metastable, or unstable *Q*-balls. Absolutely stable *Q*-balls are stable

quantum mechanically as well as classically; metastable *Q*-balls decay into free particle quanta, but are stable under small fluctuations; whereas unstable *Q*-balls, sometimes called *Q*-clouds [67], decay into lower energy *Q*-balls or free particle quanta.

E. Virial theorem

Derrick's theorem restricts the existence of static nontrivial scalar field solutions in terms of a number of spatial dimensions. For example, in a real scalar field theory, nontrivial solutions exist only in one dimension, e.g. the Klein-Gordon kink. *Q*-balls (or any nontopological solitons), however, avoid this constraint because they are time-dependent (stationary) solutions [11,12]. We can easily show this and, in doing so, obtain useful information about the scaling properties of the *Q*-balls as a function of dimensionality as well as the ratio between the surface and potential energies. Following [12], we begin by scaling the *Q*-ball ansatz Eq. (13) using a one-parameter family $r \rightarrow \alpha r$, while keeping Q fixed. Defining a surface energy $\mathcal{S} \equiv \int_{V_D} \frac{1}{2}\sigma'^2$ and a potential energy $\mathcal{U} \equiv \int_{V_D} U$, and recalling that the charge satisfies $Q = I\omega$, we see that the energy of the *Q*-ball, Eq. (10), becomes

$$E_Q = \mathcal{S} + \mathcal{U} + \frac{Q^2}{2I}. \tag{30}$$

Now, under the scaling $r \rightarrow \alpha r$, $E_Q \rightarrow E'_Q$ where $\frac{\partial E'_Q}{\partial \alpha}\big|_{\alpha=1} = 0$ because the *Q*-ball solutions are the extrema (minima) of E_Q. Evaluating this, we obtain the virial relation relating $\mathcal{U}$ and $\mathcal{S}$,

$$D\mathcal{U} = -(D-2)\mathcal{S} + D\frac{Q^2}{2I} \geq 0 \Rightarrow Q^2 \geq Q_{\min}^2, \tag{31}$$

where we have used our earlier notation, $U \geq 0$, for any values of σ and defined the minimum charge (corresponding to $\mathcal{U} = 0$) as $Q_{\min}^2 \equiv \frac{2I(D-2)}{D}\mathcal{S} > 0 \Leftrightarrow D > 2$. Since Q is taken as real and positive, no conditions appear for $D = 1, 2$. Notice this does not mean that one- and two-dimensional *Q*-balls do not exist, as can be seen from Eqs. (19) and (23). The case of $Q = 0$ recovers Derrick's theorem, showing no time-independent solutions for $D \geq 2$ [12]. Using $\mathcal{S} = \frac{DQ^2}{2I}(D - 2 + D\frac{\mathcal{U}}{\mathcal{S}})^{-1}$ from Eq. (31), the characteristic slope $E_Q/\omega Q$ becomes

$$\frac{E_Q}{\omega Q} = 1 + \left(D - 2 + D\frac{\mathcal{U}}{\mathcal{S}}\right)^{-1}. \tag{32}$$

Let us consider three cases: (i) $\mathcal{U} \gg \mathcal{S}$, (ii) $\mathcal{U} \simeq \mathcal{S}$, and (iii) $\mathcal{U} \ll \mathcal{S}$. They lead to predictions for the ratio of the *Q*-ball energy E_Q to the energy contribution from the charge ωQ:

$$\frac{E_Q}{\omega Q} \simeq \begin{cases} 1 & \text{for (i)} \\ \frac{2D-1}{2(D-1)} & \text{for (ii)} \\ \frac{D-1}{D-2} & \text{for (iii).} \end{cases} \tag{33}$$

All of the Q-balls in the range of ω are classically stable because the terms E_Q/Q monotonically increase as a function of ω; see Eqs. (28) and (33). The first case (i) corresponds to the extreme thin- and thick-wall limits $\omega \simeq \omega_\mp$, as we will see. In the second case (ii), the potential energy is of the same order as the surface energy which means $\mathcal{S}$ and $\mathcal{U}$ have equally virialized. This case will turn out to be that of the thin-wall limit for DVPs when the surface effects are included.

Suppose $\mathcal{S}/\mathcal{U} = $ const over the large range of ω within the existence condition Eq. (23), except $\omega \simeq \omega_+$ where $E_Q/\omega_+ Q \simeq 1$. We can find an approximate threshold value ω_a for a Q-ball to be absolutely stable using Eqs. (25) and (33):

$$\frac{\omega_a}{m} \simeq \begin{cases} 1 & \text{for (i)} \\ \frac{2(D-1)}{2D-1} & \text{for (ii)} \\ \frac{D-2}{D-1} & \text{for (iii).} \end{cases} \tag{34}$$

Roughly speaking, Q-balls are classically and absolutely stable if $\omega < \omega_a$ because of Eqs. (26), (28), and (33). These approximations can and will be justified by our numerical results. We will find that the virial relation is a powerful tool enabling us to find appropriate values of ω_a as opposed to the rather complicated computations we will have to adopt in the next section. We should point out a caveat in this argument; the assumption we are making here, that most of the Q-balls have an identical energy ratio $\mathcal{S}/\mathcal{U}$ over a range of ω, does of course rely on the specific form of the potential. We have to remind the readers that the virial relation Eq. (31) gives only the relation between $\mathcal{S}$ and $\mathcal{U}$, and states the presence of the minimum charge $Q_{\min}$ if the system allows the time-dependent (Q-ball) solutions Eq. (13) to exist.

III. THIN- AND THICK-WALL APPROXIMATIONS

In this section we will obtain approximate solutions for Q-balls in D dimensions based on the well-known thin- and thick-wall approximations for the radial profiles $\sigma(r)$ of the fields. Moreover, we will show how we can then use these results to verify the solutions we obtained in the previous section for $E_Q/\omega Q$ in Eq. (33). Further, we will then be able to test the solutions against detailed numerical solutions in Sec. IV. We start with two simple ansätze for the radial profiles, a steplike function for the thin-wall case $\omega \simeq \omega_-$ and a Gaussian function for the thick-wall case $\omega \simeq \omega_+$. In both cases we will evaluate S_ω, Q, E_Q, as well as the conditions for classical and absolute stability before modifying the ansätze. Following that, we will repeat the same calculations using our more physically motivated ansätze via the Legendre transformation technique de-

scribed in Eq. (17). Let us comment briefly on the form of the potential. We will see that in the thin-wall limit $\sigma_0 \simeq \sigma_+$ with our modified ansatz, although, in principle, we do not have to restrict ourselves to particular potentials, we will not be able to investigate cases where the effective potential is extremely flat; hence we will have to limit our investigation to situations where this is not the case. In the thick-wall limit $\omega \simeq \omega_+$, we have to restrict our analysis to the case of polynomial potentials of the form

$$U(\sigma) = \frac{1}{2}m^2\sigma^2 - A\sigma^n + \sum_{p>n} B_p \sigma^p \tag{35}$$

where $n \geq 3$, with the nonlinear couplings $A > 0$ and $B_p > 0$ to ensure the existence of Q-ball solutions. We expect the thin-wall approximation to be valid for general Q-ball potentials in which the Q-ball contains a lot of charge, with $\omega^2 \simeq \omega_-^2 \geq 0$. In this limit we can define a positive infinitesimal parameter, $\epsilon_\omega \equiv -U_\omega(\sigma_+) \simeq \frac{1}{2} \times (\omega^2 - \omega_-^2)\sigma_+^2 \geq 0$, and the effective mass around a "false" vacuum is given by $\mu^2 \equiv \frac{d^2 U_\omega}{d\sigma^2}\big|_{\sigma_+}$. The other extreme case corresponds to the thick-wall limit which is valid for Q-balls containing a small amount of charge, and it satisfies $\omega^2 \simeq \omega_+^2 = m^2$. For later convenience, in this limit, we define a positive infinitesimal parameter, $m_\omega^2 = m^2 - \omega^2 \geq 0$.

A. Thin-wall approximation for $D \geq 2$
1. Steplike ansatz $\omega \simeq \omega_-$

As a first step, we review the standard results in the thin-wall approximation originally obtained by Coleman [1]. Adopting a steplike ansatz for the profile, we write

$$\sigma(r) = \begin{cases} \sigma_0 & \text{for } r < R_Q \\ 0 & \text{for } R_Q \leq r, \end{cases} \tag{36}$$

where R_Q and σ_0 will be defined in terms of the underlying parameters, by minimizing the Q-ball energy. We can easily calculate S_ω, Q, and E_Q:

$$S_\omega = \left(U_0 - \frac{1}{2}\omega^2\sigma_0^2\right)V_D, \qquad Q = \omega\sigma_0^2 V_D,$$
$$E_Q = \frac{1}{2}\frac{Q^2}{\sigma_0^2 V_D} + U_0 V_D \tag{37}$$

where $U_0 \equiv U(\sigma_0)$ and $V_D = V_D(r = R_Q)$. Note that Eq. (37) satisfies the Legendre transformation results, Eq. (17), as we would have hoped. Since the ansatz Eq. (36) neglects the surface effects, we are working in the regime $\mathcal{U} \gg \mathcal{S}$ in Eq. (33). Therefore we should be able to reproduce the result $E_Q \simeq \omega Q$ with this solution. To see this, we note that the two terms in E_Q are the contributions from the charge and potential energies. These two contributions virialize since E_Q is extremized with respect to V_D for a fixed charge Q, i.e. $\partial E_Q/\partial V_D|_Q = 0$, and hence

$V_D = Q\sqrt{1/(2\sigma_0^2 U_0)}$. This then fixes R_Q because we know, for a $(D-1)$-sphere, $V_D = \frac{R_Q^D}{D}\Omega_{D-1}$ where $\Omega_{D-1} \equiv \int d\Omega_{D-1} = \frac{2\pi^{D/2}}{\Gamma(D/2)}$. Substituting $V_D = Q\sqrt{1/(2\sigma_0^2 U_0)}$ into E_Q [the third equation in Eq. (37)] and minimizing E_Q with respect to σ_0, we obtain

$$E_Q = Q \cdot \min\left(\sqrt{\frac{2U_0}{\sigma_0^2}}\right) = Q\omega_- = \omega_-^2 \sigma_+^2 V_D \qquad (38)$$

where we have used Eq. (23) in which $\omega_-^2 = \min(\frac{2U_0}{\sigma_0^2})|_{\sigma_0=\sigma_+}$. Thus we recover Eq. (33) in the limit $\mathcal{U} \gg \mathcal{S}$. Finally, we remind the reader that we have obtained the minimized energy E_Q with respect to $V_D(R_Q)$ and σ_0 in the extreme limit $\omega = \omega_-$ where we find

$$\sigma_0 = \sigma_+. \qquad (39)$$

Equation (39) implies that the particle spends a lot of "time" around σ_+ because the effective potential $-U_\omega$ around σ_+ is "flat." Note that Q and E_Q are proportional to the volume V_D in Eqs. (37) and (38) just as they are for ordinary matter; in this case Coleman called it Q-matter [1].

2. The modified ansatz $\sigma_0 \simeq \sigma_+$

Having seen the effect of an infinitely thin wall, it is natural to ask what happens if we allow for a more realistic case where the wall has a thickness associated with it? Modifying the previous steplike ansatz to include this possibility [30,68] will allow us to include surface effects [1,9,10] and provide applicability for a wider range of ω than in the steplike case. Using the results, we will examine the two different types of potentials, DVPs and NDVPs, which lead to the different cases of Eq. (33).

Following [30], the modified ansatz is written as

$$\sigma(r) = \begin{cases} \sigma_+ - s(r) & \text{for } r < R_Q \\ \bar{\sigma}(r) & \text{for } R_Q \le r \le R_Q + \delta \\ 0 & \text{for } R_Q + \delta < r, \end{cases} \qquad (40)$$

where as before the core size R_Q, the core thickness δ, the core profile $s(r)$, and the shell profile $\bar{\sigma}(r)$ will be obtained in terms of the underlying parameters by extremizing S_ω in terms of a degree of freedom R_Q. Continuity of the solution demands that we smoothly continue the profile at $r = R_Q$, namely, $\sigma_+ - s(R_Q) = \bar{\sigma}(R_Q)$ and $-s'(R_Q) = \bar{\sigma}'(R_Q)$.

We expand U_ω to leading order around σ_+, to give $U_\omega(\sigma) \sim -\epsilon_\omega + \frac{1}{2}\mu^2 s^2$ where $s(r) = \sigma_+ - \sigma(r)$. In terms of our mechanical analogy, the particle will stay around σ_+ for a long time. Once it begins to roll off the top of the potential hill, the damping due to friction [$\propto (D-1)/r$] becomes negligible and the particle quickly reaches the origin. Therefore, we can naturally assume

$$R_Q \gg \delta \qquad (41)$$

where δ is the core thickness. We know that $\sigma'(0) = -s'(0) = 0$, $s'(R_Q) \neq 0$, and $s'(r) > 0$. Using Eq. (19), the core profile $s(r)$ for $r < R_Q$ satisfies the Laplace equation:

$$s'' + \frac{D-1}{r}s' - \mu^2 s = 0 \qquad (42)$$

whose solution is

$$s(r) = r^{(1-(D/2))}(C_1 I_{(D/2)-1}(\mu r) + C_2 K_{(D/2)-1}(\mu r)) \qquad (43)$$

where I and K are, respectively, growing and decaying Bessel functions, and C_1 and C_2 are constants. Since $s(0)$ is finite and $s'(r) > 0$, this implies that $C_2 := 0$. Since $I_\nu(z) \sim z^\nu/2\Gamma(\nu+1)$ for small $z = \mu r$ and $\nu \neq -1, -2, -3\ldots$, then $s(0)$ is finite:

$$s(0) \sim C_1 \frac{\mu^{D/2-1}}{2\Gamma(D/2)} = \sigma_+ - \sigma_0 \qquad (44)$$

which gives a relation between C_1 and σ_0. Also, the analytic solution is regular at $r = 0$: $s'(0) \simeq 0$. For large $r \sim R_Q$, Eq. (43) leads to

$$\frac{s'}{s} \simeq \mu - \frac{D-2}{r} \rightarrow \mu, \qquad (45)$$

where we are assuming

$$\mu \gg 1/R_Q \qquad (46)$$

and have used the approximation $I_\nu(z) \sim \frac{e^z}{\sqrt{2\pi z}}$ for large $z \equiv \mu r$. As already mentioned, we note that this result is not strictly valid for extremely flat potentials, i.e. $\mu \simeq 1/R_Q$, because the expansion is only valid for $z \equiv \mu r \gg 1$. We will therefore only be applying it to the cases where the effective potential is not very flat.

Turning our attention to the shell regime, $R_Q \le r \le R_Q + \delta$. Considering the "friction" term in Eq. (19), we see that it becomes less important for large r compared to the first and third terms in Eq. (42), because

$$\left|\frac{D-1}{R_Q}s'(R_Q)\right| \simeq \left|\frac{D-1}{\mu R_Q}\mu^2 s(R_Q)\right| \ll \mu^2 s(R_Q)$$

$$\simeq s''(R_Q) \simeq \left|\frac{dU_\omega}{ds}\right|_{r=R_Q} \qquad (47)$$

where we have made use of Eqs. (45) and (46). Imposing continuity conditions, namely, $\sigma_+ - s(R_Q) = \bar{\sigma}(R_Q)$, $-s'(R_Q) = \bar{\sigma}'(R_Q)$, Eq. (19) without the friction term becomes

$$\frac{d^2\bar{\sigma}}{dr^2} - \frac{dU_\omega}{d\sigma}\bigg|_{\bar{\sigma}} = 0, \qquad (48)$$

where $\bar{\sigma}(r)$ is defined as being the solution to Eq. (48).

With the condition $\bar{\sigma}(R_Q) = \sigma_+ - s(R_Q)$ and Eq. (44), we find $\bar{\sigma}(R_Q) = \sigma_+ - \sqrt{\frac{2}{\pi} \frac{\Gamma(D/2)(\sigma_+ - \sigma_0)e^{\mu R_Q}}{(\mu R_Q)^{(D-1)/2}}}$. For the thin-wall limit $\sigma_0 \simeq \sigma_+$, we obtain $\bar{\sigma}(R_Q) \sim \sigma_+ - \Delta$ where Δ is an infinitesimal parameter which satisfies $\sigma_+ \gg \Delta$. Therefore

$$\bar{\sigma}(R_Q) \gg s(R_Q). \tag{49}$$

Although Eq. (18) does not hold exactly, the "total energy," $\frac{1}{2}(\frac{d\bar{\sigma}}{dr})^2 - U_\omega \sim 0$ with Eq. (18), is effectively conserved with the radial pressure p_r vanishing outside the Q-ball core. This fact implies that the surface and effective potential energies virialize with equal contributions, $\mathcal{S}_{\text{shell}} \simeq \mathcal{U}_{\text{shell}} - \frac{1}{2}\omega Q_{\text{shell}}$ where we have introduced shell and core regimes defined by $X_{\text{core}} = \Omega_{D-1} \int_0^{R_Q} dr r^{D-1} \cdots$ and $X_{\text{shell}} = \Omega_{D-1} \int_{R_Q}^{R_Q+\delta} dr r^{D-1} \cdots$ for some quantity X. Using $\sigma' < 0$ and the condition $\bar{\sigma}(R_Q + \delta) = 0$, the thickness of the Q-ball can be written as $\delta(\omega) = \int_0^{\bar{\sigma}(R_Q)} \frac{d\sigma}{\sqrt{2U_\omega}}$. Since δ is real and positive, we have to impose

$$\bar{\sigma}(R_Q) < \sigma_-, \tag{50}$$

recalling that $U_\omega(\sigma_-) = 0$ for $\sigma_- \neq 0$.

With the use of Eq. (17), we turn our attention to extremizing the Euclidean action S_ω in Eq. (11) for the degree of freedom R_Q. Using the obtained value R_Q, we will differentiate S_ω with respect to ω to obtain Q as in Eq. (16), which leads us to the Q-ball energy E_Q as in Eq. (10) and the characteristic slope $E_Q/\omega Q$. For convenience, we split S_ω into the core part S_ω^{core} for $r < R_Q$ and the shell part S_ω^{shell} for $R_Q \leq r \leq R_Q + \delta$ using Eq. (40). Using $V_D = \frac{R_Q^D}{D}\Omega_{D-1} \gg \partial V_D \equiv R_Q^{D-1}\Omega_{D-1} \gg \partial^2 V_D \equiv R_Q^{D-2}\Omega_{D-2}$ and Eqs. (42) and (45), we find

$$S_\omega^{\text{core}} = -V_D \cdot \epsilon_\omega + \partial V_D \cdot \left(\frac{1}{2}\mu s^2(R_Q)\right)$$
$$- \partial^2 V_D \cdot \left(\frac{\Omega_{D-1}}{\Omega_{D-2}} \frac{(D-2)}{\mu} \frac{1}{2}\mu s^2(R_Q)\right) \tag{51}$$

where the first term, ϵ_ω, in Eq. (51) comes from the effective potential energy, while the second and third terms arise from the surface energy. Since ϵ_ω is an infinitesimal parameter in the other thin-wall limit $\omega \simeq \omega_-$, it gives

$$\mathcal{U}_{\text{core}} \simeq \frac{1}{2}\omega Q_{\text{core}}. \tag{52}$$

The effective potential energy balances the surface energy in the shell [see Eq. (48)]; therefore, by introducing definition $T \equiv \int_0^{\bar{\sigma}(R_Q)} d\sigma\sqrt{2U_\omega}$, we see that

$$S_\omega^{\text{shell}} = \Omega_{D-1} \int_0^{\bar{\sigma}(R_Q)} d\sigma r^{D-1}\sqrt{2U_\omega(\sigma)}$$
$$\lesssim \Omega_{D-1}(R_Q + \delta)^{D-1}T \tag{53}$$

$$\to \partial V_D \cdot T + \partial^2 V_D \cdot \left(\frac{\Omega_{D-1}}{\Omega_{D-2}}(D-1)\delta \cdot T\right)$$
$$+ \mathcal{O}\left(R_Q^{D-1}, \frac{R_Q^2}{\delta^2}\right) \cdot T, \tag{54}$$

where we have used the fact that the integrand has a peak at $r = R_Q + \delta$ in the second relation of Eq. (53) [69], and Taylor-expanded $(R_Q + \delta)^{D-1}$ in going from Eq. (53) to Eq. (54) because of our approximation equation (41). Combining both expressions (51) and (54), we obtain

$$S_\omega = S_\omega^{\text{core}} + S_\omega^{\text{shell}} \tag{55}$$

$$\simeq -\epsilon_\omega \cdot V_D + \tau \cdot \partial V_D + h \cdot \partial^2 V_D \tag{56}$$

where $\tau \equiv T + \frac{1}{2}\mu s^2(R_Q)$. Note that while in τ, T contains the equally virialized surface and effective potential energies from the shell, the second term $\frac{1}{2}\mu s^2(R_Q)$ contains a surface energy term from the core. Moreover, we have defined $h \equiv \frac{\Omega_{D-1}}{\Omega_{D-2}}[(D-1)\delta \cdot T - \frac{(D-2)}{\mu}\frac{1}{2}\mu s^2(R_Q)]$ which is negligible compared to τ because of the assumptions, Eqs. (41) and (46). Therefore, we will take into account only the first two terms in S_ω, Eq. (56). It is also important to realize that

$$\tau = \int_0^{\bar{\sigma}(R_Q)} d\sigma\sqrt{2U_\omega} + \int_{\bar{\sigma}(R_Q)}^{\sigma_+} d\sigma\sqrt{2U_{\omega_-}}$$
$$\to \int_0^{\sigma_+} d\sigma\sqrt{2U_{\omega_-}} = \text{const} \tag{57}$$

which is independent of ω and D in the limit of $\omega \to \omega_-$, where we have used the other thin-wall limit $\omega \simeq \omega_-$. Our modified ansatz is not only valid in the extreme limit $\omega = \omega_-$ but also in the limit $\omega \sim \omega_-$ as long as τ depends on ω "weakly." Note that the condition of Eq. (50) also ensures that τ is positive and real. In addition, the second term in Eq. (57) is negligible compared to the first term, i.e.

$$\mathcal{S}_{\text{shell}} \simeq \mathcal{U}_{\text{shell}} - \frac{1}{2}\omega Q_{\text{shell}} \gg \mathcal{S}_{\text{core}} \tag{58}$$

because of $\sigma_+ \sim \bar{\sigma}(R_Q)$; see Eq. (49).

We can make progress by using the Legendre transformation of Eq. (17), which implies that we need to find the extrema of S_ω with fixed ω, i.e. $\frac{\partial S_\omega}{\partial R_Q} = 0$. This is equivalent to the virialization between ϵ_ω and τ. Then one can compute the core radius,

$$R_Q = (D-1)\frac{\tau}{\epsilon_\omega}. \tag{59}$$

Note that this implies that one-dimensional thin-wall Q-balls do not exist due to the positivity of R_Q. By using Eqs. (17), (56), and (59), we can compute the desired quantities to compare with the results we obtained using the steplike ansatz, in particular, Eqs. (37) and (38), and we can confirm that the classical stability condition Eq. (27) is satisfied:

$$S_\omega \simeq \frac{\tau}{D} \partial V_D = \frac{\epsilon_\omega}{D-1} V_D > 0, \qquad Q(\omega) \simeq \omega \sigma_+^2 V_D,$$
(60)

$$E_Q \simeq \omega^2 \sigma_+^2 V_D + \frac{\tau}{D} \partial V_D$$
(61)

$$\simeq \omega Q \left[\frac{2D-1}{2(D-1)} - \frac{\omega_-^2}{2(D-1)\omega^2} \right],$$
(62)

$$\frac{\omega}{Q} \frac{dQ}{d\omega} \simeq 1 - \frac{D\omega^2\sigma_+^2}{\epsilon_\omega} \simeq -\frac{D\omega^2\sigma_+^2}{\epsilon_\omega} < 0.$$
(63)

We can see the virialization between τ and ϵ_ω for the second and third terms in Eq. (60). As in Eq. (38), the first term of E_Q, in Eq. (61), is a combination of an energy from the charge and potential energy from the core throughout the volume, while the new second term $\frac{\tau}{D}$, called the surface tension, represents the equally virialized surface and effective potential energies from the shell as in Eq. (58). In the limit $\omega \simeq \omega_-$, ϵ_ω becomes zero which implies Eq. (52), as we saw. We have also seen $\mathcal{S}_{\text{shell}} \gg \mathcal{S}_{\text{core}}$. Using $\mathcal{U} = \mathcal{U}_{\text{core}} + \mathcal{U}_{\text{shell}}$, $\mathcal{S} = \mathcal{S}_{\text{core}} + \mathcal{S}_{\text{shell}} \sim \mathcal{S}_{\text{shell}}$, and Eqs. (52) and (58), we obtain

$$\mathcal{U} \sim \mathcal{S} + \omega_- Q$$
(64)

which we will use shortly. Since the characteristic function, E_Q/Q, increases monotonically as a function of ω and $S_\omega > 0$, i.e. $\frac{d}{d\omega}(\frac{E_Q}{Q}) > 0$ or Eq. (63), the classical stability condition (27) and (28) is satisfied without specifying any detailed potential forms. However, the physical properties of the finite thickness thin-wall Q-balls do depend on the vacuum structures of the underlying potential. To demonstrate this we consider two cases of NDVPs with $\omega_- \neq 0$ and DVPs with $\omega_- = 0$ (see red solid lines in Fig. 1). Suppose that the thin-wall Q-balls have identical features over a large range of ω; we can find the approximate threshold frequency ω_a using Eqs. (25) and (33) as we assumed when we obtained Eq. (34).

3. NDVPs

This type of potential reproduces the results we obtained in Eq. (38) corresponding to the regime $\mathcal{U} \gg \mathcal{S}$ which corresponds to the existence of Q-matter in that the charge and energy are proportional to the volume V_D due to the negligible surface tension in Eq. (61). Hence, the modified ansatz Eq. (40) can be simplified into the original steplike ansatz Eq. (37) with negligible surface effects in the extreme limit $\omega = \omega_-$. To see that, we need to recall the definition of ω_- in Eq. (21). We can realize that μ is the same order as ω_- except for the case of $\omega_- = 0$. Using $\mu \sim \omega_-$, we can show that $\frac{1}{2}\omega Q \gg \mathcal{S}_{\text{core}} \sim \frac{1}{2}\mu s^2(R_Q)\partial V_D$ where we have used Eqs. (46) and (49). Using Eqs. (52) and (58) and $\frac{1}{2}\omega Q \gg \mathcal{S}_{\text{core}}$ which we

just showed, we can obtain the desired result $\mathcal{U} \gg \mathcal{S}$. Similarly, Eq. (62) in the limit $\omega \simeq \omega_-$ simplifies to give $\frac{E_Q}{\omega Q} \sim 1$ which is the result of Eq. (33) with $\mathcal{U} \gg \mathcal{S}$. Using Eqs. (25), (33), and (62), we can also find the critical value ω_a for absolute stability,

$$\frac{\omega_a}{m} = \frac{D-1}{2D-1}\left(1 + \sqrt{1 + \frac{(2D-1)}{(D-1)^2}\frac{\omega_-^2}{m^2}}\right).$$
(65)

Finally, thin-wall Q-balls in NDVPs are classically stable without the need for the detailed potential forms; however, the absolute stability condition for $\omega \sim \omega_-$ depends on the spatial dimensions D and on the mass m.

4. DVPs

For the case of the presence of degenerate minima where $\omega_- = 0$, since $\epsilon_\omega = \frac{1}{2}\omega^2\sigma^2$, we immediately see from Eq. (61) that

$$\frac{E_Q}{\omega Q} \simeq \frac{2D-1}{2(D-1)}$$
(66)

which reproduces Eq. (33) for the case of $\mathcal{S} \sim \mathcal{U}$. As in NDVPs, we know Eq. (64) in the limit $\omega \simeq \omega_-$, but the second term $\omega_- Q$ becomes zero in the present potentials. It follows that $\mathcal{U}_{\text{core}} \simeq 0$ and $\mathcal{U}_{\text{shell}} \simeq \mathcal{S}_{\text{shell}} \gg \mathcal{S}_{\text{core}}$, and hence $\mathcal{S} \sim \mathcal{U}$. In other words, most of the Q-ball energy is stored within the shell. In addition, the charge Q and energy E_Q are not scaled by the volume, which implies that the modified ansatz does not recover the simple ansatz as opposed to NDVPs. In particular, we find that $Q = \frac{\Omega_{D-1}\sqrt{2(D-1)\tau}}{D\sigma_+}R_Q^{(D-1/2)} \propto R_Q^{(D-1/2)}$, $E_Q = \frac{2D-1}{D}\Omega_{D-1}\tau R_Q^{D-1} \propto R_Q^{D-1}$. A nice check of our general results follows by writing E_Q in terms of the charge Q by eliminating R_Q between the two expressions. This gives $E_Q \propto Q^{2(D-1)/(2D-1)}$ which reproduces the three-dimensional results obtained in [30].

Finally, let us recap the key approximations and conditions we have made in this modified ansatz. They are Eqs. (41), (46), (50), and (57). We believe that the estimates we have arrived at for the thin-wall Q-balls are valid as long as the core size is much larger than the shell thickness, the effective potential is not too flat around σ_+, the core thickness δ and surface tension τ/D are positive and real, and τ is insensitive to both ω and D. With the extreme limit $\omega \to \omega_-$, the Q-balls in DVPs recover the simple steplike ansatz, while the ones in NDVPs do not. One-dimensional Q-balls do not support thin-wall approximation due to the absence of the friction term in Eq. (19).

B. Thick-wall approximation for $\omega^2 \simeq \omega_+^2$, i.e. $m_\omega \to 0$

1. Gaussian ansatz

As we have started with the simple steplike ansatz in the thin-wall approximation, a Gaussian function is a simple approximate profile to describe the thick-wall Q-balls [12]. Using a Gaussian ansatz

$$\sigma(r) = \sigma_0 \exp\left(-\frac{r^2}{R^2}\right), \qquad (67)$$

we will extremize S_ω with respect to σ_0 and R with fixed ω, instead of minimizing E_Q with fixed Q. Notice that the slope $-\sigma'/\sigma$ becomes $2r/R^2$, which is linearly proportional to r, and the solution is regular at $r = 0$: $\sigma'(0) = 0$. Neglecting higher order terms B_p in Eq. (35) with Eq. (67), one can obtain straightforwardly

$$Q = \left(\frac{\pi}{2}\right)^{D/2} \omega \sigma_0^2 R^D, \qquad (68)$$

$$S_\omega \simeq \left(\frac{1}{2} m_\omega^2 + \frac{D}{R^2} - A\sigma_0^{n-2}\left(\frac{2}{n}\right)^{D/2}\right) \frac{Q}{\omega},$$

$$E_Q \simeq \left[\frac{1}{2}(m^2 + \omega^2) + \frac{D}{R^2} - A\sigma_0^{n-2}\left(\frac{2}{n}\right)^{D/2}\right] \frac{Q}{\omega}. \qquad (69)$$

Equation (17) can be easily checked in Eqs. (68) and (69). The first and last terms in Eq. (69) are the potential energy terms. The second energy term comes from the charge energy, and the surface energy term appears in the third term. By finding the extrema of S_ω with respect to σ_0 with $\frac{\partial S_\omega}{\partial \sigma_0} = 0$, it defines the underlying parameter σ_0 as

$$\sigma_0 = \left[\left(m_\omega^2 + \frac{2D}{R^2}\right)\frac{1}{nA}\left(\frac{n}{2}\right)^{D/2}\right]^{1/n-2}$$

$$\to \left(\frac{m_\omega^2}{2A}\right)^{1/n-2} \sim \sigma_- \qquad (70)$$

where we have neglected the surface term and used the approximation $D/2 \simeq \mathcal{O}(1)$ in the second relation of Eq. (70). Then we can check that the Gaussian ansatz naturally satisfies the other thick-wall limit $\sigma_0 \simeq \sigma_-$ and that the higher order terms B_p in Eq. (35) are negligible. Using the first relation of Eq. (70), one needs to extremize S_ω with respect to another degree of freedom R with $\frac{\partial S_\omega}{\partial R} = 0$ which determines R:

$$R = \sqrt{\frac{2(2 - D)}{m_\omega^2}} \geq 0. \qquad (71)$$

The reality condition on R implies that the Gaussian ansatz is valid only for $D = 1$. The width of the Gaussian function R in Eq. (71) becomes very large in the thick-wall limit $m_\omega \to 0$; thus we can justify that the surface terms in Eqs. (69) and (70) are negligible. Therefore, we are looking at the regime $\mathcal{U} \gg \mathcal{S}$ which should lead us to $E_Q \simeq \omega Q$ as in the first case of Eq. (33). To do this for $D = 1$, we

substitute Eq. (70) into Q, E_Q, S_ω:

$$Q = \sqrt{\frac{\pi}{2}} \omega \sigma_0^2 R, \qquad S_\omega = \left(\frac{1}{2} - \frac{1}{n}\right)\frac{2m_\omega^2 Q}{\omega} > 0, \quad (72)$$

$$\frac{E_Q}{\omega Q} = \left(\frac{1}{2} + \frac{1}{n}\right) + \left(\frac{1}{2} - \frac{1}{n}\right)\left(\frac{2m^2}{\omega^2} - 1\right) \to 1 \qquad (73)$$

where we have considered the thick-wall limit $\omega \simeq m$ in the second relation of Eq. (73). We can check Eq. (33) and the analytic continuation Eq. (25). In the same limit, the Euclidian action becomes an infinitesimally small positive value: $S_\omega \to 0^+$.

Using the second relation σ_0 in Eqs. (70) and (71), one can find

$$\frac{\omega}{Q}\frac{dQ}{d\omega} \simeq 1 - \frac{\omega^2}{m_\omega^2}\left(\frac{4}{n-2} - 1\right) \to -\frac{\omega^2}{m_\omega^2}\left(\frac{4}{n-2} - 1\right) \leq 0 \qquad (74)$$

where we have used the fact that m_ω is a positive infinitesimal parameter in the limit $\omega \simeq \omega_+$ going from the first relation to the second one. Equation (74) shows that the classical stability condition clearly depends on the nonlinear power n in the potential Eq. (35): $n \leq 6$. This is contradictory because Eq. (73) gives $\frac{d}{d\omega}\left(\frac{E_Q}{Q}\right) \to -1 + \frac{4}{n}$ which implies $n \leq 4$ for the other classical stability condition using Eq. (28). We will shortly see that this contradiction between Eqs. (27) and (28) is an artefact of the Gaussian ansatz. Moreover, our conclusion should state that the Gaussian approximation is valid only for $D = 1$. These awkward consequences are improved with the following physically motivated ansatz.

2. The modified ansatz

Having considered the case of the simple Gaussian ansatz following the spirit of [12], we found some problems for the classical stability. To fix these, we need a more realistic ansatz [11,30,38,39,49]. To do this, we drop an explicit detailed profile to describe thick-wall Q-balls and rescale the field profile so as to work in dimensionless units while extracting out the explicit dependence on ω from the integral in S_ω. As in the thin-wall approximation with the modified ansatz, we will again make use of the technique equation (17) to obtain other physical quantities from S_ω.

We begin by defining $\sigma = a\tilde{\sigma}$ and $r = b\tilde{r}$ with a and b which will depend on ω. Substituting them into Eq. (11) with the potential Eq. (35), we obtain

$$S_\omega = \int d\Omega_{D-1} \int d\tilde{r}\tilde{r}^{D-1} b^D \left\{\frac{1}{2}\left(\frac{a}{b}\right)^2 \tilde{\sigma}'^2 + \frac{1}{2} a^2 m_\omega^2 \tilde{\sigma}^2 - Aa^n \tilde{\sigma}^n + \sum_{p>n} B_p a^p \tilde{\sigma}^p\right\}, \qquad (75)$$

$$= b^D \left(\frac{a}{b}\right)^2 \Omega_{D-1} \int d\tilde{r}\tilde{r}^{D-1} \frac{1}{2}\left\{\tilde{\sigma}'^2 + \tilde{\sigma}^2 - \tilde{\sigma}^n\right.$$

$$\left. + \sum_{p>n} B_p b^2 a^{p-2}\tilde{\sigma}^p\right\}, \tag{76}$$

$$\simeq m_\omega^{4/(n-2)-D+2} A^{-2/(n-2)}\Omega_{D-1}S_n \tag{77}$$

with the rescaled action $S_n = \int d\tilde{r}\tilde{r}^{D-1}(\frac{1}{2}\tilde{\sigma}'^2 + \tilde{U})$ with $\tilde{U} = \frac{1}{2}\tilde{\sigma}^2 - \frac{1}{2}\tilde{\sigma}^n$, and we have neglected the higher order terms involving B_p. In going from Eq. (75) to Eq. (76) we have set the coefficients of the first three terms in the brackets to be unity in order to explicitly remove the ω dependence from the integral in S_ω. In other words, we have set $\frac{1}{2}(\frac{a}{b})^2 = \frac{1}{2}a^2 m_\omega^2 = Aa^n$. This implies $a = (\frac{m_\omega^2}{2A})^{1/(n-2)} = \sigma_-$ and $b = m_\omega^{-1}$. Crucially, S_n is independent of ω, and is positive definite [11,30,49]. Adopting the powerful approach developed in Eq. (17), given S_ω, we can differentiate it to obtain Q and then use the Legendre transformation to obtain E_Q. This is straightforward and yields

$$Q(\omega) = \omega m_\omega^{4/(n-2)-D}\left(\frac{4}{n-2} - D + 2\right)A^{-2/(n-2)}\Omega_{D-1}S_n$$

$$\propto m_\omega^{4/(n-2)-D}, \tag{78}$$

$$E_Q = m_\omega^{4/(n-2)-D}\left[m_\omega^2\right.$$

$$\left. + \omega^2\left(\frac{4}{n-2} - D + 2\right)\right]A^{-2/n-2}\Omega_{D-1}S_n, \tag{79}$$

$$= \omega Q\left[1 + \frac{m_\omega^2}{\omega^2}\left(\frac{4}{n-2} - D + 2\right)^{-1}\right] \to \omega Q. \tag{80}$$

The first term in Eq. (80) is the energy contributed by the charge, while the second term is dominated by the effective potential energy; hence $\mathcal{U} \gg \mathcal{S}$. Therefore, we can also recover the result $E_Q \simeq \omega Q$ in the thick-wall limit $\omega \simeq \omega_+$ as we would expect from Eq. (33) when $\mathcal{U} \gg \mathcal{S}$. Since Q and E_Q should be positive definite, it places the constraint [49]

$$D < \frac{4}{n-2} + 2. \tag{81}$$

With the condition Eq. (81), it is easy to see that $S_\omega \to 0^+$ in the thick-wall limit $\omega \simeq \omega_+$ where $m_\omega^2 \to 0^+$. There is another constraint emerging from the need for the solution to be classically stable:

$$\frac{\omega}{Q}\frac{dQ}{d\omega} \simeq 1 - \frac{\omega^2}{m_\omega^2}\left(\frac{4}{n-2} - D\right)$$

$$\to -\frac{\omega^2}{m_\omega^2}\left(\frac{4}{n-2} - D\right) \leq 0, \tag{82}$$

$$\Leftrightarrow D \leq \frac{4}{n-2} \tag{83}$$

which coincides with Eq. (74) in the case of $D = 1$. Notice that the modified ansatz is valid not only for $D = 1$ but also for $D < \frac{4}{n-2} + 2$ in Eq. (81). For $D = 3$ this result matches that of [30]. The classical stability condition, Eq. (83), is consistent with the need for Q and E_Q to be finite. Equation (83) is more restrictive than Eq. (81). Furthermore, we should check the relation Eq. (28) for the characteristic function E_Q/Q in terms of ω. It follows that $\frac{d}{d\omega}\left(\frac{E_Q}{Q}\right) \simeq 1 - 2(\frac{4}{n-2} - D + 2)^{-1} \geq 0$, which requires the same condition as Eq. (83). With this fact and Eq. (80), it implies that thick-wall Q-balls satisfy the conditions for both classical and absolute stabilities. Moreover, it also reproduces the previous results in [70], for the case of $D = 2$ and $n = 4$, $p = 6$ (6th order potential). Unlike the Gaussian ansatz Eq. (67), our modified ansatz now shows consistent results between Eqs. (27) and (28).

Let us remark on the validity of our analysis following [49]. In this section we have used a modified ansatz which has involved a rescaling of σ and r in such a way as to leave us with a dimensionless action S_n. There are restrictions on our ability to do this, as first pointed out in [49] for the case of $D = 3$. We can generalize this to our D-dimensional case. Given that the Q-ball solutions extremize S_n, we may rescale r or σ introducing a one-parameter rescaling, $r \to \alpha r$ or $\sigma \to \lambda\sigma$, which will deform the original solution. Defining $X(\alpha) \equiv S_n[\alpha r, \sigma(\alpha r)]$ and $Y(\lambda) \equiv S_n[\lambda\sigma(r)]$, we impose the condition that the action S_n is extremized when $\alpha = \lambda = 1$, which implies $\frac{dX}{d\alpha}|_{\alpha=1} = 0 = \frac{dY}{d\lambda}|_{\lambda=1}$. It is possible to show that these conditions imply that consistent solutions require the same condition as Eq. (81). The three-dimensional case leads to the result $n < 6$, as originally obtained in [30]. The particular choice of $n = 4$, which we will investigate shortly, implies $D < 4$ for the validity of our thick-wall approximation with the modified ansatz. Moreover, thick-wall Q-balls become classically unstable for $D \geq 3$, as can be seen from Eq. (83).

What have we learned from extending the ansatz beyond the Gaussian one? We have seen that they lead to different results. For instance, the Gaussian ansatz has a contradiction for the classical stability analysis even for $D = 1$, whereas the solutions based on the modified ansatz are valid for D, which satisfies Eq. (81), and give consistent results, Eq. (83), for classical stability.

As we will see in the next section, our numerical results in which we obtain the full Q-ball solution support the modified ansätze for both thin- and thick-wall cases.

IV. NUMERICAL RESULTS

In this section we obtain numerical solutions for Q-balls using the polynomial potential in Eq. (35), including only one higher order term:

$$U(\sigma) = \tfrac{1}{2}m^2\sigma^2 - A\sigma^n + B\sigma^p, \tag{84}$$

where $A > 0$, $B > 0$, $p > n > 2$. We shall confirm the results obtained analytically using the modified ansätze for both the thin- and thick-wall Q-balls. Recall that $U_\omega(\sigma) = U(\sigma) - \tfrac{1}{2}\omega^2\sigma^2$, with $U_\omega(\sigma_-) = 0$, and σ_+ marks the maximum of the effective potential $-U_\omega$ where $\sigma_+ \neq 0$. For a particular case $p = 2(n-1)$, we find

$$\sigma_-(\omega) = \left(\frac{A - \sqrt{A^2 - 2Bm_\omega^2}}{2B}\right)^{1/(n-2)},$$
$$\sigma_+(\omega) = \left(\frac{An + \sqrt{(An)^2 - 4Bpm_\omega^2}}{2Bp}\right)^{1/(n-2)}. \tag{85}$$

Also, for convenience, we set

$$\omega_+ = m = 1, \qquad \omega_- = \sqrt{1 - \frac{A^2}{2B}} \geq 0 \Leftrightarrow A \leq \sqrt{2B}, \tag{86}$$

where we recall that the definitions of ω_+ and ω_- are $\omega_+^2 \equiv \frac{d^2U}{d\sigma^2}|_{\sigma=0} = m^2$ and $U_{\omega_-}(\sigma_+) \equiv 0$. Setting $\omega_- = 0$ in Eq. (86) implies that $U(\sigma)$ in Eq. (84) has degenerate vacua at $\sigma = 0, \pm\sigma_+$, while the original potential U does not have degenerate vacua with $\omega_- \neq 0$. In this section, we shall consider two examples of the potential U, which can be seen as the red solid lines in Fig. 1. The DVP on the left has $\omega_- = 0$ ($A = \sqrt{2B}$) and the NDVP on the right has $\omega_- = 0.5$ ($A = \sqrt{3B/2}$). In order to determine actual values for A and B, we define $\sigma_+(\omega_+) = 1$ and set $n = 4$, $p = 6$ for both cases; hence $A = \frac{4}{3}$, $B = \frac{8}{9}$ in DVP and $A = 1$, $B = \frac{2}{3}$ in NDVP. Figure 1 also includes plots of the effective potentials for various values of ω.

A. Numerical techniques and parameters

To obtain the Q-ball profile, we need to know the initial "position" $\sigma_0 = \sigma(r = 0)$. This is done using a shooting method, whereby we initially guess at a value of σ_0, then solve Eq. (19) for the Q-ball profile; depending on whether we overshoot or undershoot the required final value of σ, we modify our guess for σ_0 and try again. Throughout our simulations, we need to specify the following three small parameters, ϵ, ξ, η which, respectively, determine our simulation size $r_{\max}$, the radius at which we can match the analytic and numerical solutions (R_{ana}), and the core size R_Q. The smoothly continued profile is computed up to $r = R_{\max}$.

1. Shooting method

Let us consider an effective potential $-U_\omega$ which satisfies the Q-ball *existence condition*, Eq. (23). We have to initially guess σ_0 subject to it being in the appropriate

region $\sigma_- \leq \sigma_0 < \sigma_+$. For example, it might be $\sigma_G^0 = \frac{\sigma_+ + \sigma_-}{2}$. There are then three possibilities: the particle could overshoot, undershoot, or shoot properly. The last case is unlikely unless we are really "lucky." If it overshoots, then we would find $\sigma(r_O) < 0$ at some time r_O. If that were to happen, we could update σ_G^0 to $\sigma_G^1 = \frac{\sigma_G^0 + \sigma_-}{2}$ as our next guess. On the other hand, if it undershoots, the "velocity" of the particle might be positive at some time r_U, $\sigma'(r_U) > 0$. If that were to happen, we might update σ_G^0 to $\sigma_G^1 = \frac{\sigma_+ + \sigma_G^0}{2}$ as our next guess. After repeating the same procedures, say, N times, we obtain the finely tuned initial position $\sigma_0 \simeq \sigma_G^N$ as our true value. To be compatible with numerical errors, our numerical simulation should be stopped with an appropriate accuracy parametrized by ϵ:

$$\epsilon > \sigma(r_U = r_{\max}) > 0 \tag{87}$$

where $r_{\max}$ is the size of our simulations, and ϵ measures the numerical accuracy where a small value of ϵ corresponds to good numerical accuracy. Unfortunately, the final profiles still have small numerical errors for large r. To compensate for these errors, the profiles should continue to the analytical ones smoothly at some point $r = R_{\mathrm{ana}}$.

2. Matching analytic and numerical solutions at R_{ana}

For large r, the Q-ball equation (19) can be reduced to

$$\sigma'' + \frac{D-1}{r}\sigma' - m_\omega^2\sigma = 0. \tag{88}$$

The analytic solution becomes

$$\sigma(r) \sim E\sqrt{\frac{\pi}{2m_\omega}}r^{-(D-1/2)}e^{-m_\omega r} \Leftrightarrow -\frac{\sigma'}{\sigma} \sim \frac{D-1}{2r} + m_\omega \tag{89}$$

where E is a constant which is determined later. Note that we have used the fact that the modified Bessel function of the second kind has the relation $K_\mu(r) \simeq \sqrt{\frac{\pi}{2r}}e^{-r}$ for large r and any real number μ. In order to smoothly continue to the analytic profile Eq. (89) at the continuing point R_{ana}, the following condition is required using the second relation of Eq. (89):

$$\left|\frac{D-1}{2r} + m_\omega + \frac{\sigma'_{\mathrm{num}}}{\sigma_{\mathrm{num}}}\right| < \xi \tag{90}$$

where a parameter ξ should be relatively small. Hence we can find the appropriate profile in the whole space,

$$\sigma(r) = \begin{cases} \sigma_{\mathrm{num}}(r) & \text{for } r < R_{\mathrm{ana}} \\ \sigma_{\mathrm{num}}(R_{\mathrm{ana}})(\frac{R_{\mathrm{ana}}}{r})^{(D-1)/2}e^{-m_\omega(r-R_{\mathrm{ana}})} & \text{for } R_{\mathrm{ana}} \leq r \leq R_{\max}, \end{cases} \tag{91}$$

where we have computed E using Eq. (89), and our simulations are carried out up to $r = R_{max}$.

3. Core size and thickness of thin-wall Q-balls

Using Eq. (45), we can define the core size $r = R_Q$ and the numerical thickness δ_{num} by the slope $-\sigma'/\sigma$ with the following condition:

$$\left| \left(\frac{D - 2}{r} - \mu \right) \left(\frac{\sigma_+ - \sigma}{\sigma} \right) + \frac{\sigma'_{num}}{\sigma_{num}} \right| < \eta, \quad (92)$$

$$\delta_{num} \equiv R_{ana} - R_Q. \quad (93)$$

Notice that the definition of δ_{num} is different from the definition in Eq. (41), where $\delta(\omega) = \int_0^{\bar{\sigma}(R_Q)} \frac{d\sigma}{\sqrt{2U_\omega}}$.

4. Numerical parameters

We have run our code in two different regimes of ω for both DVP and NDVP because the profiles for large ω are needed to look into larger simulation size r_{max} compared to the ones for small ω. Because of numerical complications, we do not conduct our simulations near the extreme thin-wall limit, i.e. $\omega \simeq \omega_-$. However, by solving close to the thin-wall limit, our numerical results for $\sigma_0 \simeq \sigma_+$ and $R_Q \gg \delta_{num}$ allow us to recover the expected properties of thin-wall Q-balls with the modified ansatz Eq. (40). Finally, our results presented here correspond to the particular sets of parameters summarized in Table I.

B. Stationary properties in DVP and NDVP

We devote a large part of this section to justifying the previously obtained analytical results in the thin- and thick-wall approximations by obtaining the appropriate numerical solutions.

1. Profiles with our numerical algorithm

In the top two panels of Fig. 2 the two red lines (one dotted and one with circles) show the numerical slopes $-\sigma'/\sigma$ for the case of $D = 3$ for two values of ω. These are then matched to the analytic profiles (green dotted

lines) in order to achieve the full profile as given in Eq. (91). Recall that we expect, in general, for all values of ω, the analytic fits to be accurate for large r, the numerical fits to be most accurate for small r, and for there to be an overlap region where they are both consistent with each other as seen in Fig. 2. We have also plotted in dot-dashed purple lines our analytic fits, Eq. (92), for the slopes of the thin-wall cores from $r = 0.5$. We should remind the reader that this fit only really works for the case of small ω because we are dealing with thin-wall Q-balls. Notice that it is clear from the purple lines that the core sizes cannot be determined by this technique for the case $\omega = 0.9 \simeq \omega_+$.

The bottom two panels show the full profiles satisfying Eq. (91) for arbitrary D up to $D = 5$. We have been able to obtain the Q-ball profiles in the whole parameter space ω except for the extreme thin-wall region $\omega \simeq \omega_-$. Both DVP and NDVP Q-balls have profiles with similar behaviors in that, as the spatial dimension increases, so does their core size.

2. Criteria for the existence of a thin-wall Q-ball with core size R_Q

The top and middle panels of Fig. 3 show the numerical results for $\sigma_0(\omega)$ and δ_{num}/R_Q against ω for a number of spatial dimensions D. For the case of $D \geq 3$ it is clear from the top panels that the Q-balls are well described by the thin-wall result Eq. (85) for most values of ω, with the range increasing as D increases. The case of $D = 2$ is less clear; it appears to asymptote onto the line. We believe there is a solution that exists for that case for small values of ω. An important point is that for the approximation to be valid we are working in the regime $\delta_{num}/R_Q < 1$, which can be seen to be true from the middle panels (again, we believe the case of $D = 2$ is heading below the line $\delta_{num}/R_Q = 1$ for small ω).

These results are consistent with our analytic solutions for finite thickness Q-balls given by Eq. (40), subject to the criteria $\sigma_0 \simeq \sigma_+$ and $R_Q \gtrsim \delta_{num}$, even though $\omega \sim \omega_+$.

For $D = 1$ we see in the top panels that σ_0 exactly matches σ_- (the orange dot-dashed lines). The bottom two panels in Fig. 3 show the core sizes R_Q of thin-wall

TABLE I. The numerical parameters in DVP (top) and in NDVP (bottom).

DVP					
ω	ϵ	r_{max}	R_{max}	ξ	η
0.38–0.73	4.0×10^{-2}	30	200	8.0×10^{-3}	1.0×10^{-1}
0.73–0.999 99	1.0×10^{-5}	40	200	8.0×10^{-3}	1.0×10^{-1}

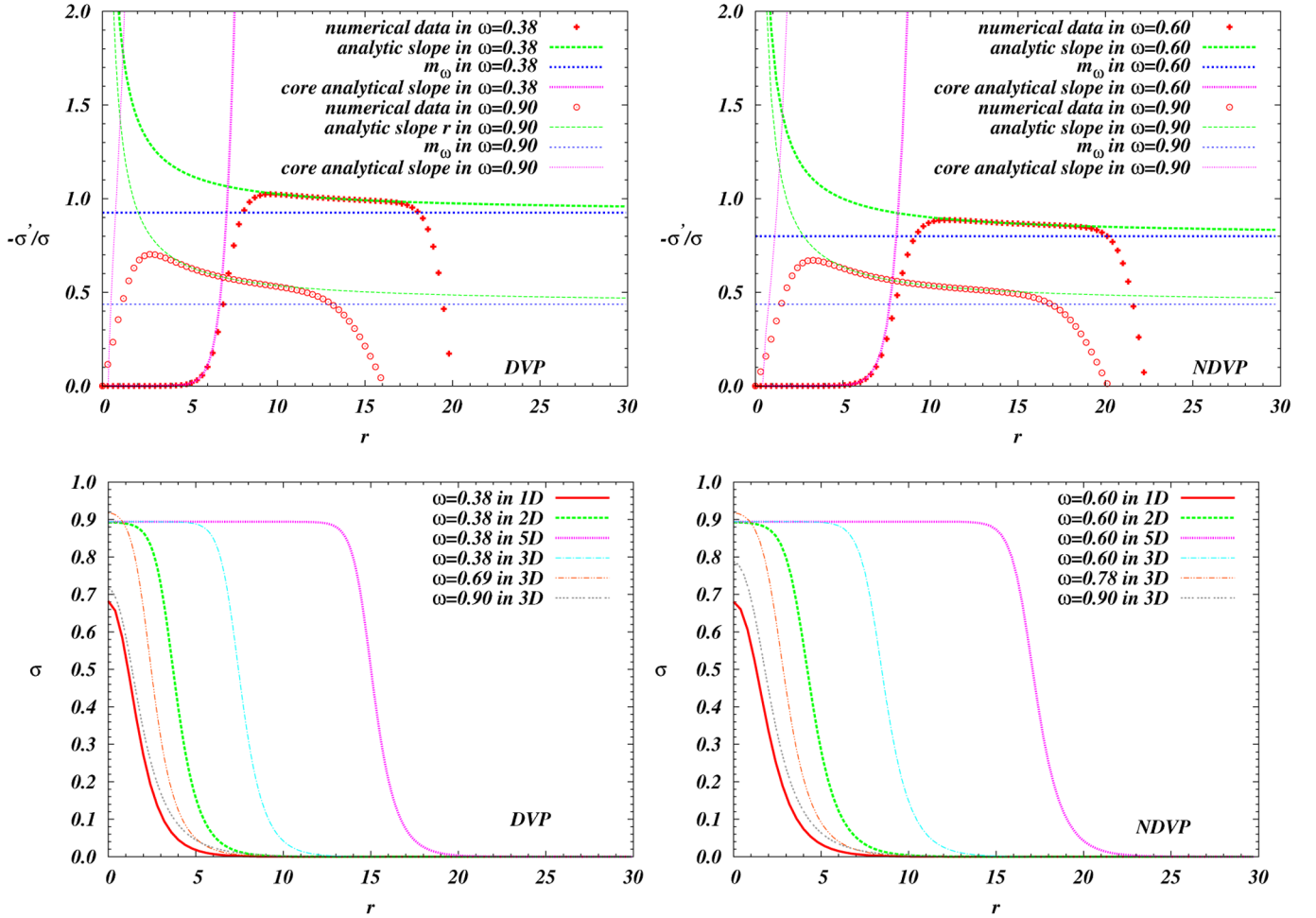| NDVP					
ω	ϵ	r_{max}	R_{max}	ξ	η
0.60–0.85	3.0×10^{-3}	30	200	8.0×10^{-3}	1.0×10^{-1}
0.85–0.999 99	1.0×10^{-5}	50	200	8.0×10^{-3}	1.0×10^{-1}

FIG. 2 (color online). The top two panels show the numerical slopes $-\sigma'/\sigma$ for the case of $D = 3$ for two values of ω for both DVP (left panel) and NDVP (right panel). The red (one dotted and one with circles) lines show the numerical slopes, and the green dotted lines with two different widths show the corresponding analytic solutions. The purple dot-dashed lines with two different widths show the analytic fits for the core profiles. The bottom two panels show the full Q-ball profile as described in Eq. (91) for a number of values of ω and D. Note how the core size increases with D.

Q-balls which satisfy our criterion Eq. (92). Recall that R_Q in Eq. (59) is a function of ω, assuming τ depends on ω weakly; thus we plot the numerical core sizes, comparing them with our analytical approximations for DVP and NDVP, respectively:

$$R_Q^{\mathrm{DVP}} \simeq \frac{2(D-1)\tau_{\mathrm{num}}}{\omega^2}; \qquad R_Q^{\mathrm{NDVP}} \simeq \frac{2(D-1)\tau_{\mathrm{num}}}{(\omega^2 - \omega_-^2)} \quad (94)$$

where the parameter τ_{num} is computed numerically (see Table II). The presented numerical core sizes match excellently with the analytical fittings over a wide range of ω. Some numerical errors appear around $\omega \simeq \omega_+$ since we cannot determine the thick-wall cores with this technique; see the top two panels in Fig. 2. Table II shows analytical and numerical values of τ using Eq. (57) and the above fitting technique. We confirm that the values of τ [part of the surface tension τ/D in Eq. (61)] are nearly constant,

depending slightly on D. Therefore, the assumptions we made for thin-wall Q-balls are valid as long as $\sigma_0 \simeq \sigma_+$ and $R_Q \gtrsim \delta_{\mathrm{num}}$.

3. Configurations

Figure 4 illustrates the configurations of charge density ρ_Q (top panels) and energy density ρ_E (bottom panels), in both DVP (left panels) and NDVP (right panels). Each of the DVP energy densities around $\omega \sim \omega_-$ has a spike within the shells, while those spikes are not present in NDVP. The presence of spikes can contribute to the increase in surface energy $\mathcal{S}$, which accounts for the different observed ratio for $\mathcal{S}/\mathcal{U}$ in the two cases, where $\mathcal{U}$ is the potential energy. Otherwise, DVP and NDVP models have similar profiles in Fig. 2. Moreover, we have numerically checked that Q-balls for $D \geq 2$ generally have positive radial pressures, whereas the $1D$ radial pressures are always zero, i.e. $\frac{1}{2}\sigma'^2 = U_\omega$ due to Eq. (15).
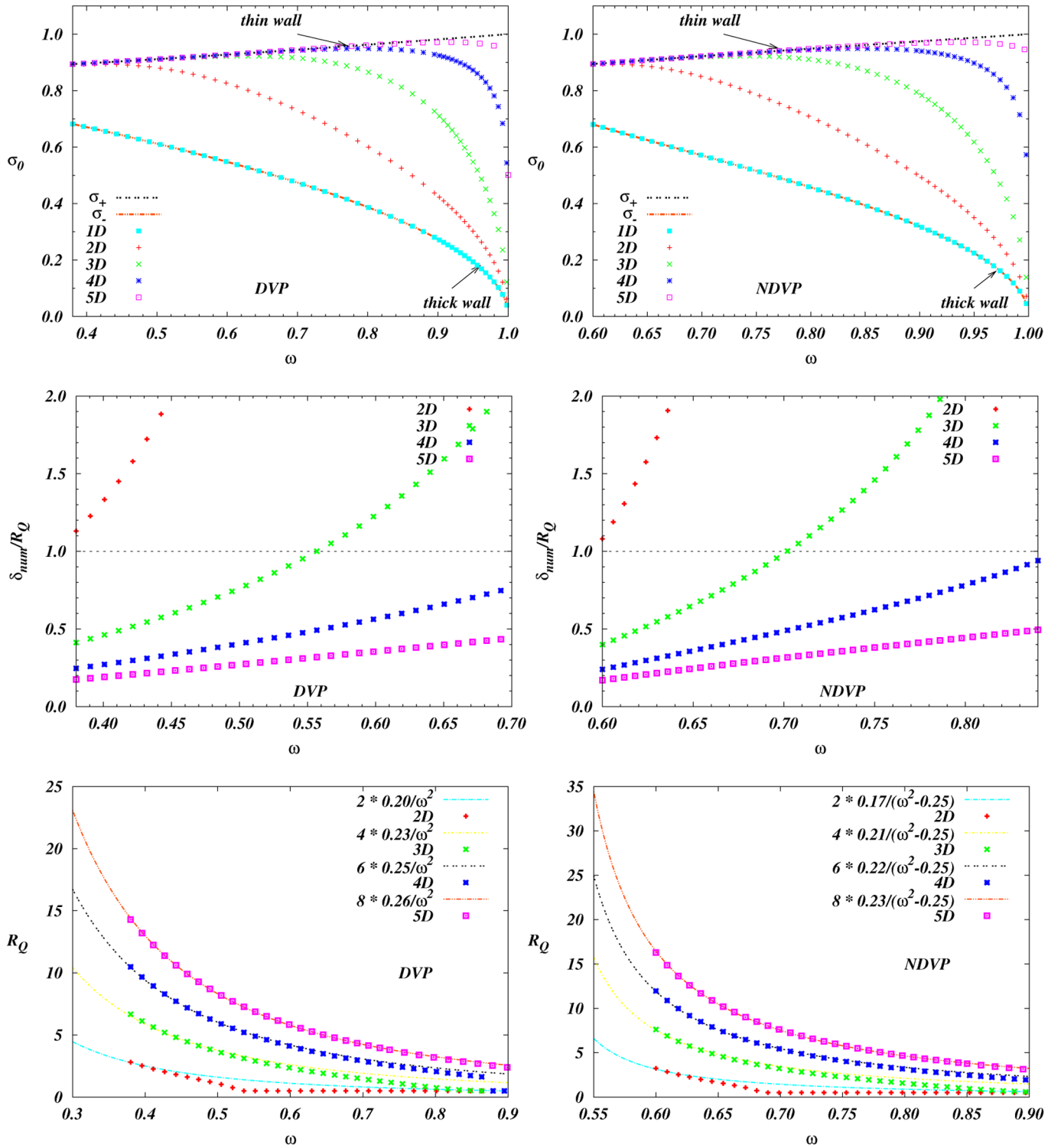
FIG. 3 (color online). The initial "positions" σ_0 (top panels), δ_{num}/R_Q (middle panels), and the core sizes $R_Q(\omega)$ (bottom panels). The top panels show $\sigma_\pm$, Eq. (85), as black and orange dot-dashed lines, respectively. The middle panels show the range of values of ω for a given value of D in which the core thickness is smaller than the core size, a crucial assumption we have to make. In the bottom panels, the analytical core sizes in Eq. (94) are plotted with the numerical ones for the following ω ranges: [0.38–0.40], [0.38–0.55], [0.38–0.60], [0.38–0.70] in DVP, and [0.60–0.62], [0.60–0.65], [0.60–0.75], [0.60–0.85] in NDVP, and for $D = 2, 3, 4, 5$, respectively. As can be seen, the fits are excellent. The range of ω values chosen has been based on the results shown in the top two panels and correspond to that range where the thin-wall Q-balls are solutions (except for $D = 2$).

TABLE II.   The values of τ_{ana} and τ_{num} in terms of D in DVP and NDVP; see Eqs. (57) and (59).

τ	τ_{ana}	2D	3D	4D	5D
DVP	0.19	0.20	0.23	0.25	0.26
NDVP	0.16	0.17	0.21	0.22	0.23

4. Virialization and characteristic slope $E_Q/\omega Q$

The top panels in Fig. 5 illustrate the ratios $\mathcal{S}/\mathcal{U}$, and the four bottom ones show the characteristic slopes of $E_Q/\omega Q$ against ω in both the thin-wall (middle panels) and thick-wall (bottom panels) limits. According to our analytic arguments, Eq. (64), we expect $\mathcal{S}/\mathcal{U} \simeq 1$ in the extreme limit $\omega \simeq \omega_- = 0$ in DVP. Similarly, we expect $\mathcal{S}/\mathcal{U} \sim 0$ in the same extreme thin-wall limit $\omega = \omega_- = 0.5$ for NDVP. The latter case corresponds to the existence of Q-matter with the simple steplike ansatz Eq. (36). Although we are unable to probe these precise regimes,

we believe the slopes of the curves indicate they are heading in the right direction. The thin-wall slopes $E_Q/\omega Q$ in the two middle panels lie nearby the analytical ones, Eqs. (62) and (66), as long as $\sigma_0 \simeq \sigma_+$ (see Fig. 3), except for the 2D cases because for $D \leq 2$ the profiles are not well fitted by thin-wall predictions. Similarly, the thick-wall slopes $E_Q/\omega Q$ in the bottom two panels agree with our analytical predictions, Eq. (80), using the modified ansatz rather than with Eq. (73) using the simple Gaussian ansatz. We have confirmed that the analytic thick-wall slopes with Eq. (80) cannot apply to higher dimensions $D \geq 4$; see Eq. (81). Around the thick-wall limit $\omega \simeq \omega_+$, the behaviors in both potentials are $\mathcal{S} \ll \mathcal{U}$ (see top panels), which implies $E_Q \simeq \omega Q$ as predicted in Eqs. (73) and (79); hence we can verify that the solutions are continued to the free particle solutions [see Eq. (25)]. Our physically motivated modified ansätze in both the thin- and thick-wall limits therefore have clear advantages over the simple ansätze in Eqs. (36) and (67).
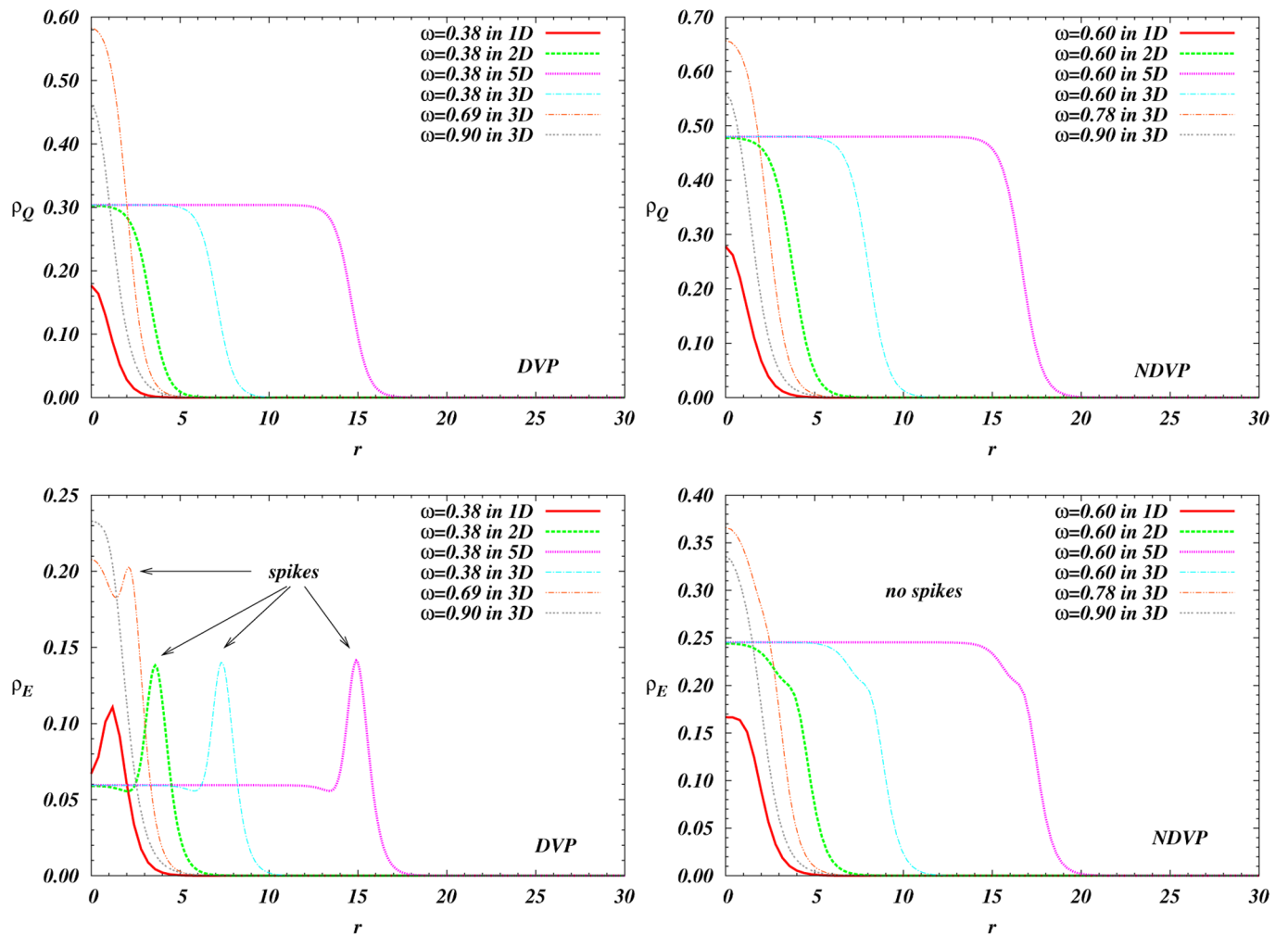

FIG. 4 (color online).   The configurations for charge density ρ_Q (top panels) and energy density ρ_E (bottom panels) computed using Eq. (14) for both DVP (left panels) and NDVP (right panels). The presence of spikes of ρ_E in DVPs contributes to their increased surface energies.
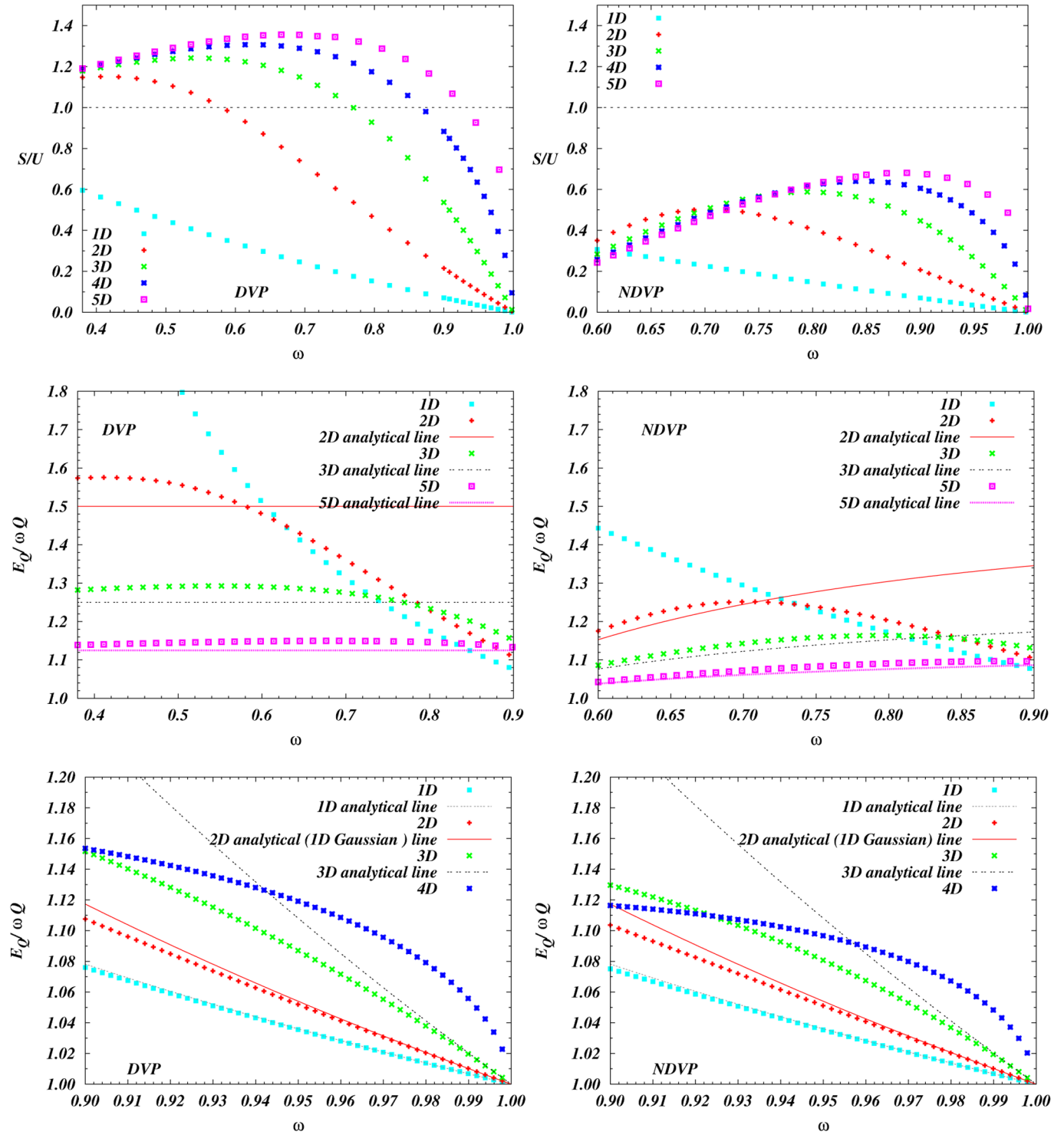
FIG. 5 (color online). The ratio of $\mathcal{S}/\mathcal{U}$ where $\mathcal{S}$ and $\mathcal{U}$ are surface and potential energies (top panels), the characteristic slope $E_Q/\omega Q$ in the thin-wall-like limit, $\omega \sim \omega_-$, with the analytic lines, Eq. (62) (middle panels), and in the thick-wall-like limit, $\omega \simeq \omega_+$ (bottom panels), with the analytic lines, Eqs. (73) and (80).

5. Q-ball stability

Figure 6 shows the classical and absolute stability lines for Q-balls. Table III indicates the approximate analytical values of ω_a derived by Eqs. (34) and (65), which can be

compared to the numerically obtained critical values ω for the stabilities denoted by ω_c, ω_s, ω_{ch}, ω_a, and ω_f in Table IV. Each of these are defined by $\frac{dQ}{d\omega}\big|_{\omega_c} = \frac{d^2 S_\omega}{d\omega^2}\big|_{\omega_s} = \frac{d}{d\omega}(\frac{E_Q}{Q})\big|_{\omega_{\text{ch}}} = 0$, $E_Q/Q|_{\omega_a} = m$, and $\frac{d\omega}{dQ}\big|_{\omega_f} = 0$, respec-
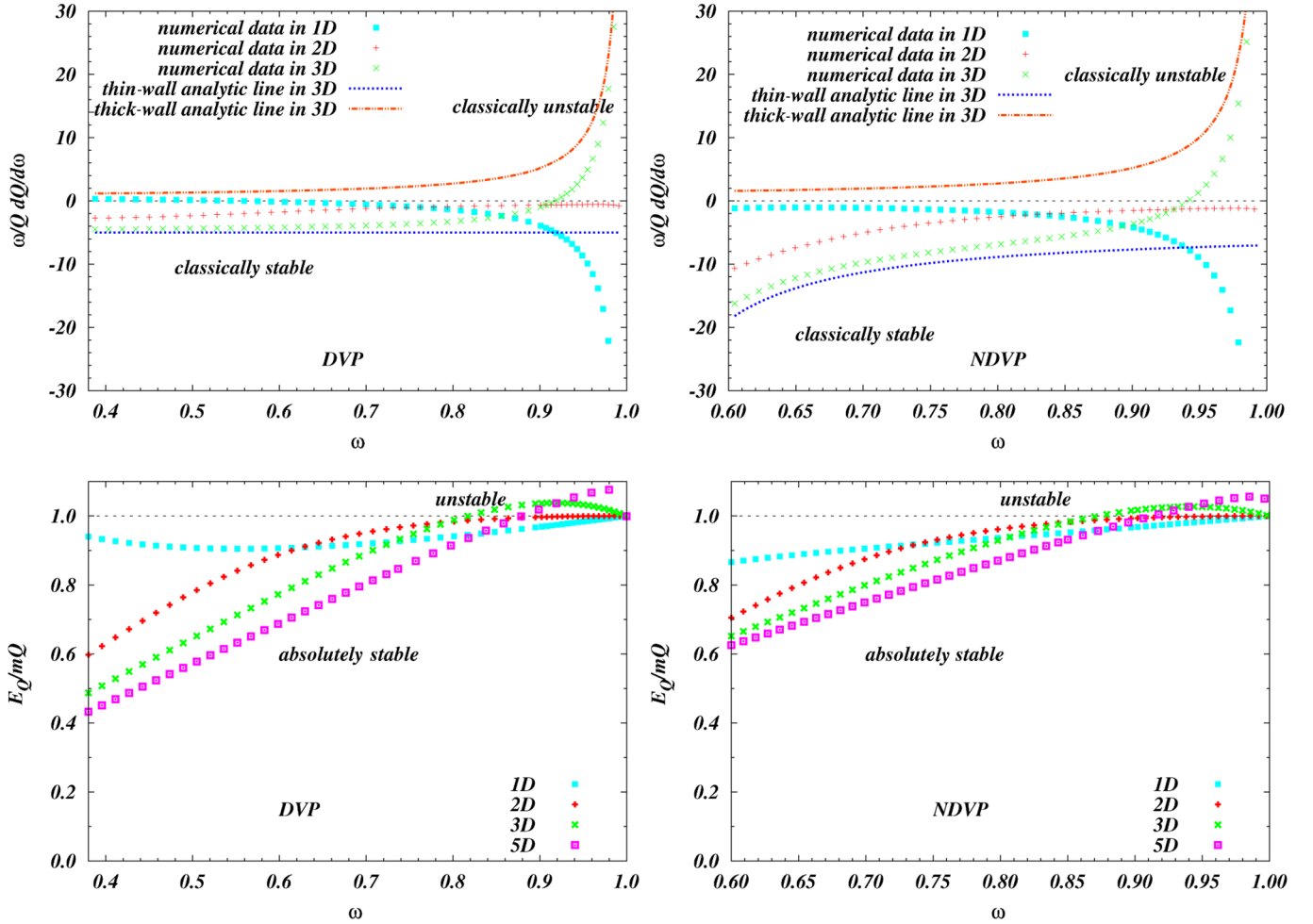
FIG. 6 (color online).   Classical stability using Eq. (27) for the top panels, and absolute stability using Eq. (26) for the bottom panels. The $3D$ analytical lines of Eqs. (63) and (83) for classical stability agree with the corresponding numerical data. Above the zero-horizontal axes in the top panels, the Q-balls are classically unstable. Similarly, Q-balls above the horizontal axis, $E_Q = mQ$, are quantum-mechanically unstable. The one-dimensional Q-balls are always classically stable. The $1D$ slopes E_Q/mQ have different behaviors depending on DVP and NDVP, unlike the other dimensional cases.

tively. The $3D$ analytical plots of $\frac{\omega}{Q}\left(\frac{dQ}{d\omega}\right)$ in the thin- and thick-wall limits, Eqs. (63) and (83), can be seen to match the corresponding numerical data in the appropriate limits of ω. We have confirmed numerically that for both DVP and NDVP cases $\omega_c = \omega_f \simeq \omega_s \simeq \omega_{\mathrm{ch}}$; see Table IV. This can be easily understood from Eqs. (27)–(29).

TABLE III.   Virial relations: ω_a in terms of space dimension D and ratio $\mathcal{S}/\mathcal{U}$; see Eq. (34).

		ω_a		
D	$\mathcal{S} \gg \mathcal{U}$	$\mathcal{S} \simeq \mathcal{U}$ or DVP	NDVP	$\mathcal{S} \ll \mathcal{U}$
3	0.50	0.80	0.86	1
4	0.67	0.86	0.90	1
5	0.75	0.89	0.92	1

Recall that Eq. (83), the polynomial potential Eq. (84) with $n = 4$, leads to the classical stability condition $D \leq 2$ for the thick-wall case. The top panels in Fig. 6 demonstrate that thick-wall Q-balls in $D \geq 3$ are classically unstable. In Table IV, one can check that the absolute stability condition is more severe than the classical one; then there are three types of Q-balls [2], as before: absolutely stable Q-balls for $\omega < \omega_a$; metastable Q-balls for $\omega_a \leq \omega \leq \omega_c$, which are not quantum-mechanically stable but classically stable, and can decay into multiple Q-balls; or unstable Q-balls for $\omega_c < \omega$.

Both DVP and NDVP analytical values ω_a in Table III agree well with the numerical ones in Table IV. Generally speaking, the higher-dimensional Q-balls are more stable classically as well as quantum mechanically. Moreover, thin-wall Q-balls are always classically stable as demonstrated in Eq. (63), but the classical stability of thick-wall

TABLE IV. The critical values for classical stability, absolute stability, and stability against fission in DVP and NDVP using Eqs. (26)–(29). The critical values are defined by $\frac{dQ}{d\omega}|_{\omega_c} = \frac{d^2 S_\omega}{d\omega^2}|_{\omega_s} = \frac{d}{d\omega}(\frac{E_Q}{Q})|_{\omega_{ch}} = 0$, $E_Q/Q|_{\omega_a} = m$, and $\frac{d\omega}{dQ}|_{\omega_f} = 0$. The numerical values of ω_a coincide with the analytic ones in Table III. We have confirmed numerically that $\omega_c = \omega_f \simeq \omega_s \simeq \omega_{ch}$.

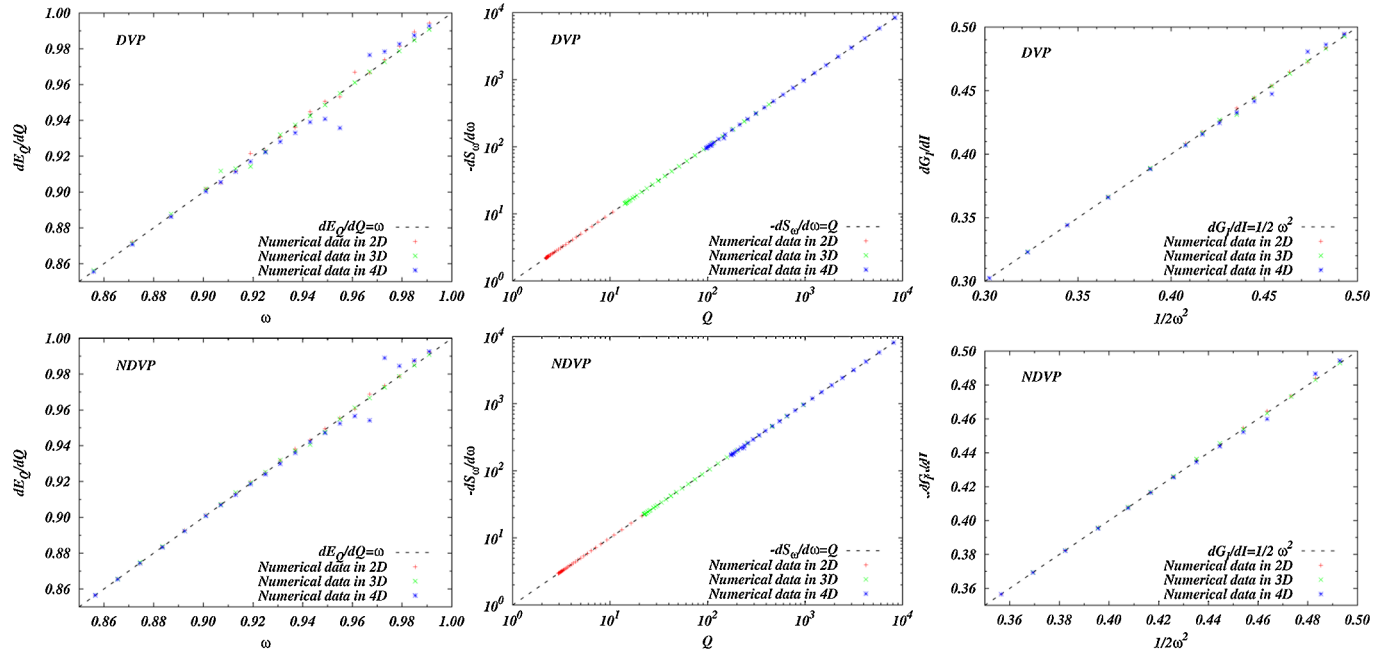|	DVP					NDVP				
D	ω_a	ω_c	ω_s	ω_{ch}	ω_f	ω_a	ω_c	ω_s	ω_{ch}	ω_f
3	0.82	0.92	0.92	0.92	0.92	0.87	0.94	0.94	0.94	0.94
4	0.86	0.96	0.96	0.96	0.96	0.89	0.97	0.97	0.97	0.97
5	0.882	0.983	0.993	0.983	0.983	0.910	0.985	0.996	0.991	0.985

FIG. 7 (color online). The Legendre relations of Eq. (16): $\frac{dE_Q}{dQ} = \omega$ (left panels), $-\frac{dS_\omega}{d\omega} = Q$ (middle panels), and $\frac{dG_I}{dI} = \frac{1}{2}\omega^2$ (right panels). Note the excellent agreement between the analytical dotted lines and the numerical data (dots).

Q-balls is model and D dependent as in Eq. (83). The one- and two-dimensional Q-balls have a much richer structure than the thin- and thick-wall Q-balls. It is a challenging task to understand their intermediate profiles [71].

6. Legendre relations

Figure 7 shows the Legendre relations: $\frac{dE_Q}{dQ}$ vs ω, $-\frac{dS_\omega}{d\omega}$ v.s Q, and $\frac{dG_I}{dI}$ vs $\frac{1}{2}\omega^2$, which can be used to check Eq. (16). We have also checked the validity of the Legendre transformations in Eqs. (10)–(12). Since the numerical results match our analytical ones, these results strengthen the validity of our analytic arguments.

V. CONCLUSION

We have numerically and analytically explored the stationary properties of a single Q-ball for an arbitrary spatial dimension D. With the time-dependent nonlinear solutions in the system, the virial theorem induces the characteristic

slopes, Eq. (33), and gives the approximate critical values for ω_a in Eq. (34) without requiring a knowledge of the detailed profiles and potential forms. By linearizing the Q-ball equation (19) or rescaling in S_ω, we have been able to consider the two limiting cases called the thin- and thick-wall Q-balls. The steplike ansatz of Eq. (36) can describe thin-wall Q-balls in the extreme limit $\omega = \omega_-$, whereas the modified ansatz Eq. (40) is applicable to $\sigma_0 \simeq \sigma_+$ which leads to a wider range of parameter space ω and of course includes the previous limit. On the other hand, the limit $\omega \simeq \omega_+$ is used to describe thick-wall Q-balls in both the Gaussian ansatz Eq. (67) and our modified ansatz for the thick-wall case.

The thin-wall approximation is valid for $D \geq 2$. Since the steplike ansatz in the thin-wall approximation does not have surface effects, the characteristic slope is simply $E_Q/\omega Q = 1$, Eq. (38). With the modified ansatz including surface effects, the classical stability for thin-wall Q-balls does not depend on D in Eq. (63), but the absolute stability condition Eq. (65) does. Throughout the analysis, we have

assumed Eqs. (41) and (46), and imposed Eq. (50) explicitly, which differs from the analysis in [30]. Without these approximations, our calculations, in particular Eqs. (53), (54), and (56), become inconsistent. The mechanical analogies and the numerical results naturally explain and validate our underlying assumptions: the core sizes of the Q-balls are much smaller than their corresponding thickness as seen in the middle two panels of Fig. 3, and the surface tension depends weakly on ω as seen in Table II. With these assumptions, thin-wall Q-balls for $\omega < \omega_a$ are absolutely stable. Moreover, the characteristic slopes coincide with those derived using the virial theorem. This follows from our analysis of the relative contributions between the potential and surface energies. The slopes have two types in either NDVPs or DVPs: NDVPs have a large energy from the charge; hence the surface energy is less effective than the potential energy. They support the existence of Q-matter in the extreme limit, $\omega = \omega_-$. DVPs, however, have negligible energy from the charge compared to surface and potential energies; thus the surface energy is well virialized with the potential energy. As seen in the lower-left panel of Fig. 4, the configurations of energy density have peaks within the shells, which contribute to the surface energy. It would be worthwhile to understand these peaks in terms of our modified ansatz. Even in the extreme thin-wall limit, the charge and energy of the Q-balls in NDVPs are not proportional to the volume, i.e. no Q-matter.

Thick-wall Q-ball solutions naturally tend to free charged and massive particle solutions, Eq. (25). With the simple Gaussian ansatz, we have extremized S_ω with respect to σ_0 and R with fixed ω, while the approaches in [12] are that E_Q is extremized with respect to only R. By extremizing with respect to 2 degrees of freedom, we are able to recover the expected results of Eqs. (70) and (73) unlike in [12]. The Gaussian ansatz, however, is valid only for $D = 1$ because of Eq. (71), and gives contradictory results for the condition for classical stability. In order to remove these drawbacks in the Gaussian ansatz, we introduced another modified ansatz and used the Legendre relations to simplify the computations of S_ω, Q, E_Q. We obtained a consistent classical stability condition Eq. (83) which depends on D and a nonlinear power n of the polynomial potential Eq. (35). Not surprisingly, our numerical results suggest that the modified ansatz is much better than the Gaussian ansatz in the bottom two panels of

Fig. 5. With the same panels, the validity condition Eq. (81) in the modified ansatz has also been confirmed numerically.

In Eqs. (34) and (65) and Table IV, the analytical and numerical results found the critical value ω_a with an assumption. The assumption says that the higher-dimensional Q-balls could be applicable to the thin-wall approximations over a wide range of values of ω. Although this statement may not hold for extremely flat potentials [35,51] because μ can be as small as $1/R_Q$ [see Eq. (46)] and the energy spectrum has the following proportionality, $E_Q \propto Q^{D/D+1}$, we believe that it may apply to other large types of Q-ball potentials. In summary, the higher-dimensional Q-balls can be simplified into the thin- and thick-wall cases, while it is more challenging and interesting to understand stationary properties of one- and two-dimensional Q-balls. For example, those Q-balls embedded in $3D$ space (called Q-strings and Q-walls) may exist in the formation of three-dimensional Q-balls [65,72].

The properties of nonthermal Q-balls can lead to different consequences compared to thermal ones, i.e. in the evolution of the Universe. The thermal effects on Q-balls induce subsequent radiation and evaporation. The Affleck-Dine condensate provides a natural homogeneous condensate with small quantum fluctuations; these fluctuations are then amplified to nonlinear objects, namely, Q-balls, if the pressure of Affleck-Dine condensates is negative. The formation, dynamics, and thermalization might have phenomenological consequences in our present Universe, e.g. gravitational waves [73] and baryon-to-photon ratio.

[1] S. R. Coleman, Nucl. Phys. **B262**, 263 (1985); **B269**, 744 (E) (1986).

[2] R. Friedberg, T. D. Lee, and A. Sirlin, Phys. Rev. D **13**, 2739 (1976).

[3] T. D. Lee and Y. Pang, Phys. Rep. **221**, 251 (1992).

[4] R. Rajaraman, *Solitons and Instantons* (North Holland, Amsterdam, 1989), 2nd reprint, 1989 edition, ISBN 13:978-0444870476.

[5] M. Dine and A. Kusenko, Rev. Mod. Phys. **76**, 1 (2003).

[6] K. Enqvist and A. Mazumdar, Phys. Rep. **380**, 99 (2003).

[7] R. Battye and P. Sutcliffe, Nucl. Phys. **B590**, 329 (2000).

[8] C. G. Callan and S. R. Coleman, Phys. Rev. D **16**, 1762 (1977).

[9] D. Spector, Phys. Lett. B **194**, 103 (1987).

[10] T. Shiromizu, T. Uesugi, and M. Aoki, Phys. Rev. D **59**, 125010 (1999).

[11] A. Kusenko, Phys. Lett. B **404**, 285 (1997).

[12] M. Gleiser and J. Thorarinson, Phys. Rev. D **73**, 065008 (2006).

[13] K. M. Lee, J. A. Stein-Schabes, R. Watkins, and L. M. Widrow, Phys. Rev. D **39**, 1665 (1989).

[14] T. S. Levi and M. Gleiser, Phys. Rev. D **66**, 087701 (2002).

[15] K. N. Anagnostopoulos, M. Axenides, E. G. Floratos, and N. Tetradis, Phys. Rev. D **64**, 125006 (2001).

[16] X. Z. Li, J. G. Hao, D. J. Liu, and G. Chen, J. Phys. A **34**, 1459 (2001).

[17] T. Shiromizu, Phys. Rev. D **58**, 107301 (1998).

[18] A. M. Safian, S. R. Coleman, and M. Axenides, Nucl. Phys. **B297**, 498 (1988).

[19] A. M. Safian, Nucl. Phys. **B304**, 392 (1988).

[20] M. Axenides, E. Floratos, and A. Kehagias, Phys. Lett. B **444**, 190 (1998).

[21] R. Jackiw, K. M. Lee, and E. J. Weinberg, Phys. Rev. D **42**, 3488 (1990).

[22] R. Jackiw and E. J. Weinberg, Phys. Rev. Lett. **64**, 2234 (1990).

[23] J. Hong, Y. Kim, and P. Y. Pac, Phys. Rev. Lett. **64**, 2230 (1990).

[24] M. Deshaies-Jacques and R. MacKenzie, Phys. Rev. D **74**, 025006 (2006).

[25] Y. Kiem, C. j. Kim, and Y. b. Kim, Phys. Lett. B **507**, 207 (2001).

[26] R. Friedberg and T. D. Lee, Phys. Rev. D **15**, 1694 (1977).

[27] R. Friedberg and T. D. Lee, Phys. Rev. D **16**, 1096 (1977).

[28] T. D. Lee and Y. Pang, Phys. Rev. D **35**, 3678 (1987).

[29] B. W. Lynn, Nucl. Phys. **B321**, 465 (1989).

[30] F. Paccetti Correia and M. G. Schmidt, Eur. Phys. J. C **21**, 181 (2001).

[31] K. M. Benson, Nucl. Phys. **B327**, 649 (1989).

[32] R. Rajaraman and E. J. Weinberg, Phys. Rev. D **11**, 2950 (1975).

[33] A. G. Cohen, S. R. Coleman, H. Georgi, and A. Manohar, Nucl. Phys. **B272**, 301 (1986).

[34] K. M. Benson, J. Bernstein, and S. Dodelson, Phys. Rev. D **44**, 2480 (1991).

[35] M. Laine and M. E. Shaposhnikov, Nucl. Phys. **B532**, 376 (1998).

[36] M. S. Volkov and E. Wohnert, Phys. Rev. D **66**, 085003 (2002).

[37] Y. Brihaye and B. Hartmann, arXiv:0711.1969.

[38] J. Shatah and W. Strauss, Commun. Math. Phys. **100**, 173 (1985).

[39] Ph. Blanchard, J. Stubbe, and L. Vzquez, Ann. Inst. Henri Poincare Phys. Theor. **47**, 309 (1987).

[40] I. L. Bogolubsky and V. G. Makhankov, Pis'ma Zh. Eksp. Teor. Fiz. **24**, 15 (1976) [JETP Lett. **24**, 12 (1976)]; **25**, 120 (1977); V. G. Makhankov, Phys. Rep. **35**, 1 (1978).

[41] M. Gleiser, Phys. Rev. D **49**, 2978 (1994).

[42] E. J. Copeland, M. Gleiser, and H. R. Muller, Phys. Rev. D **52**, 1920 (1995).

[43] S. Kasuya, M. Kawasaki, and F. Takahashi, Phys. Lett. B **559**, 99 (2003).

[44] P. M. Saffin and A. Tranberg, J. High Energy Phys. 01 (2007) 030.

[45] M. Gleiser, B. Rogers, and J. Thorarinson, Phys. Rev. D **77**, 023513 (2008).

[46] M. Hindmarsh and P. Salmi, Phys. Rev. D **77**, 105025 (2008).

[47] G. H. Derrick, J. Math. Phys. (N.Y.) **5**, 1252 (1964).

[48] M. Axenides, S. Komineas, L. Perivolaropoulos, and M. Floratos, Phys. Rev. D **61**, 085006 (2000).

[49] T. Multamaki and I. Vilja, Nucl. Phys. **B574**, 130 (2000).

[50] T. Multamaki and I. Vilja, Phys. Lett. B **484**, 283 (2000).

[51] Asko Jokinen, Ph.D. thesis [Helsinki Institute of Physics Internal Report No. HIP-2002-08], "Affleck-Dine mechanism and Q-balls along SUSY flat directions," http://ethesis.helsinki.fi/julkaisut/mat/fysik/vk/jokinen/.

[52] K. Enqvist and J. McDonald, Phys. Lett. B **425**, 309 (1998).

[53] T. Multamaki and I. Vilja, Phys. Lett. B **482**, 161 (2000).

[54] I. Affleck and M. Dine, Nucl. Phys. **B249**, 361 (1985).

[55] S. Kasuya and M. Kawasaki, Phys. Rev. D **61**, 041301 (2000).

[56] S. Kasuya and M. Kawasaki, Phys. Rev. D **62**, 023512 (2000).

[57] K. Enqvist, A. Jokinen, T. Multamaki, and I. Vilja, Phys. Rev. D **63**, 083501 (2001).

[58] T. Multamaki and I. Vilja, Phys. Lett. B **535**, 170 (2002).

[59] K. Enqvist, S. Kasuya, and A. Mazumdar, Phys. Rev. D **66**, 043505 (2002).

[60] K. M. Lee, Phys. Rev. D **50**, 5333 (1994).

[61] Vladimir A. Koutvitsky and Eugene M. Maslov, J. Math. Phys. (N.Y.) **47**, 022302 (2006).

[62] K. Griest, E. W. Kolb, and A. Massarotti, Phys. Rev. D **40**, 3529 (1989).

[63] N. H. Christ and T. D. Lee, Phys. Rev. D **12**, 1606 (1975).

[64] E. J. Copeland, K. Enqvist, P. M. Saffin, and M. I. Tsumagari (to be published).

[65] Movies demonstrating *Q*-ball dynamics have been created using the 3D software package VAPOR (www.vapor.ucar.edu), and are available at "http://www.nottingham.ac.uk/physics/research/particles/people/Mitsuo/welcome.html."

[66] V. Glaser, K. Grosse, A. Martin, and W. Thirring, in *Studies in Mathematical Physics*, edited by E. Lieb, B. Simon, and A. Wightman (Princeton University Press, Princeton, NJ, 1976), Vol. 169.

[67] M. G. Alford, Nucl. Phys. **B298**, 323 (1988).

[68] S. R. Coleman, Phys. Rev. D **15**, 2929 (1977); **16**, 1248 (1977).

[69] D. K. Hong, J. Low Temp. Phys. **71**, 483 (1988).

[70] C. j. Kim, S. Kim, and Y. b. Kim, Phys. Rev. D **47**, 5434 (1993).

[71] N. Sakai and M. Sasaki, Prog. Theor. Phys. **119**, 929 (2008).

[72] R. B. MacKenzie and M. B. Paranjape, J. High Energy Phys. 08 (2001) 003.

[73] J. Garcia-Bellido, D. G. Figueroa, and A. Sastre, Phys. Rev. D **77**, 043517 (2008).